DTNSRDC-81/081

DAVID W. TAYLOR NAVAL SHIP RESEARCH AND DEVELOPMENT CENTER

Bethesda, Maryland 20084

LIFTING-SURFACE HYDRODYNAMICS FOR DESIGN OF ROTATING BLADES

by

Terry E. Brockett

APPROVED FOR PUBLIC RELEASE: DISTRIBUTION UNLIMITED

Presented at
PROPELLERS '81 SYMPOSIUM
The Society of Naval Architects and Marine Engineers
Virginia Beach, Virginia, May 26-27, 1981

SHIP PERFORMANCE DEPARTMENT
RESEARCH AND DEVELOPMENT REPORT

October 1981

DTNSRDC-81/081

URFACE HYDRODYNAMICS FOR DESIGN OF ROTATING BLADES

MAJOR DTNSRDC ORGANIZATIONAL COMPONENTS

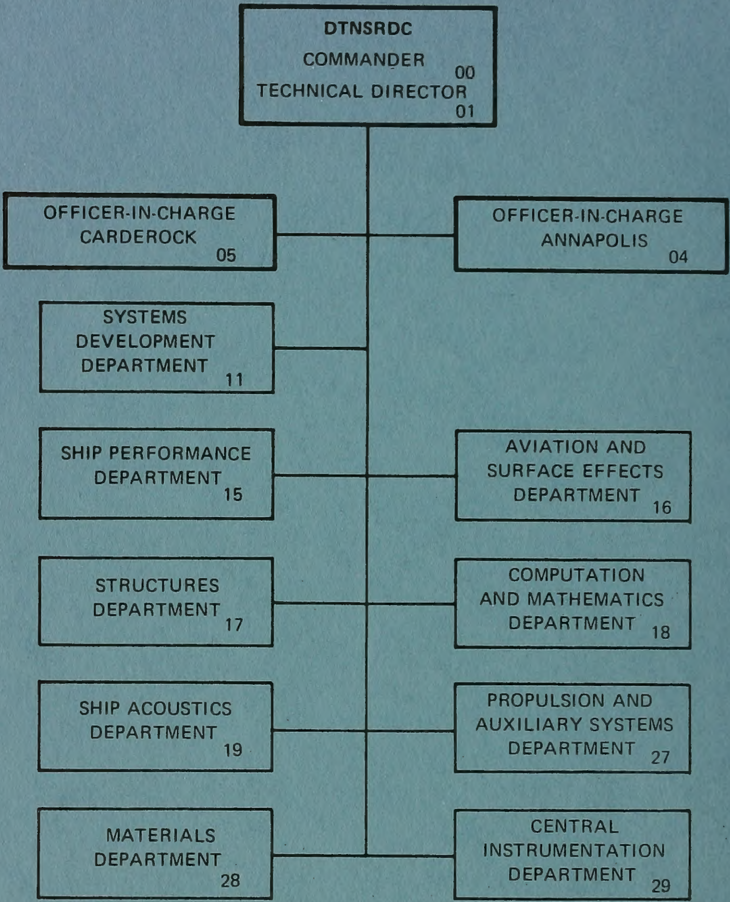

NDW-DTNSRDC 3960/43 (Rev. 11-75)
GPO 905-679

UNCLASSIFIED

SECURITY CLASSIFICATION OF THIS PAGE *(When Data Entered)*

REPORT DOCUMENTATION PAGE

READ INSTRUCTIONS BEFORE COMPLETING FORM

1. REPORT NUMBER: DTNSRDC-81/081
2. GOVT ACCESSION NO.:
3. RECIPIENT'S CATALOG NUMBER:

4. TITLE *(and Subtitle)*: LIFTING-SURFACE HYDRODYNAMICS FOR DESIGN OF ROTATING BLADES

5. TYPE OF REPORT & PERIOD COVERED: SHIP PERFORMANCE DEPT. RESEARCH AND DEVELOPMENT

6. PERFORMING ORG. REPORT NUMBER:

7. AUTHOR(s): Terry E. Brockett

8. CONTRACT OR GRANT NUMBER(s):

9. PERFORMING ORGANIZATION NAME AND ADDRESS:
David W. Taylor Naval Ship Research and Development Center
Bethesda, Maryland 20084

10. PROGRAM ELEMENT, PROJECT, TASK AREA & WORK UNIT NUMBERS:
Task Area SF43421001
Program Element 62543N
Work Unit 1500-104

11. CONTROLLING OFFICE NAME AND ADDRESS:
Naval Sea Systems Command (05R)
Ship Systems Research and Technology Group
Washington, D.C. 20362

12. REPORT DATE: October 1981

13. NUMBER OF PAGES: 31

14. MONITORING AGENCY NAME & ADDRESS *(if different from Controlling Office)*:
Naval Sea Systems Command (524)
Propulsion Line Shafting Equipment Division
Washington, D.C. 20362

15. SECURITY CLASS. *(of this report)*: UNCLASSIFIED

15a. DECLASSIFICATION/DOWNGRADING SCHEDULE:

16. DISTRIBUTION STATEMENT *(of this Report)*:

APPROVED FOR PUBLIC RELEASE: DISTRIBUTION UNLIMITED

17. DISTRIBUTION STATEMENT *(of the abstract entered in Block 20, if different from Report)*:

18. SUPPLEMENTARY NOTES:

19. KEY WORDS *(Continue on reverse side if necessary and identify by block number)*:

Marine Propeller
Propeller Research
Propulsion
Model Experiments
Propeller Theory

20. ABSTRACT *(Continue on reverse side if necessary and identify by block number)*:

Analysis and numerical results are presented for the design of a system of wide-bladed thin lifting surfaces rotating at constant angular velocity in an axisymmetric onset flow field. Blade sections may be located arbitrarily in space. General chordwise and spanwise loading functions are available as well as a variety of thickness forms. In addition to the final meanline and pitch distribution determined from a chordwise integration of

(Continued on reverse side)

DD FORM 1 JAN 73 1473 EDITION OF 1 NOV 65 IS OBSOLETE
S/N 0102-LF-014-6601

UNCLASSIFIED

SECURITY CLASSIFICATION OF THIS PAGE *(When Data Entered)*

(Block 20 continued)

an appropriate combination of geometric variables and induced velocities, additional information not available from other existing techniques includes pressure distributions and surface metrics for an orthogonal streamline coordinate system on the blade surface, as defined in the Appendix. The induced velocity field on the blades is derived from the principal value of a singular integral; the evaluation of this integral is discussed. The predictions are generally supported by experimental data. A new term in the analysis arises from a radial onset flow component and an example illustrates its importance in design. Sufficient information for manufacture is obtained for computer run times from 400 to 1200 seconds on the Burroughs 7700 high-speed computer.

TABLE OF CONTENTS

LIST OF FIGURES

LIST OF TABLES

THE SOCIETY OF NAVAL ARCHITECTS AND MARINE ENGINEERS
One World Trade Center, Suite 1369, New York, N.Y. 10048
Paper to be presented at the Propellers '81 Symposium, Virginia Beach, Virginia, May 26-27, 1981

Lifting-Surface Hydrodynamics for Design of Rotating Blades

No. 20

Terry Brockett, David Taylor Naval Ship Research and Development Center, Bethesda, MD

ABSTRACT

Analysis and numerical results are presented for the design of a system of wide-bladed thin lifting surfaces rotating at constant angular velocity in an axisymmetric onset flow field. Blade sections may be located arbitrarily in space. General chordwise and spanwise loading functions are available as well as a variety of thickness forms. In addition to the final meanline and pitch distribution determined from a chordwise integration of an appropriate combination of geometric variables and induced velocities, additional information not available from other existing techniques includes pressure distributions and surface metrics for an orthogonal streamline coordinate system on the blade surface, as defined in the Appendix. The induced velocity field on the blades is derived from the principal value of a singular integral; the evaluation of this integral is discussed. The predictions are generally supported by experimental data. A new term in the analysis arises from a radial onset flow component and an example illustrates its importance in design. Sufficient information for manufacture is obtained for computer run times from 400 to 1200 seconds on the Burroughs 7700 high-speed computer.

NOTATION

A, B	Point values in linear approximation for distance
C_D	Blade-section drag coefficient
$C_p = (p - p_\infty)/(\rho V^2/2)$	Pressure coefficient
$C_P = 2\pi Qn/(\rho V^3 \pi D^2/8)$	Power loading coefficient based on reference speed
$C_{Th} = T/(\rho V^2 \pi D^2/8)$	Thrust loading coefficient based on reference speed
$c(x_R)$	Blade-section chord length
D	Rotor diameter
D_f	Friction drag on blade section
$E(x_c, x_R) = E_c \pm E_T$	Profile shape function
$E_c(x_c, x_R)$	Meanline shape function
$E_T(x_c, x_R)$	Thickness shape function
$(\underline{e}_1, \underline{e}_2, \underline{e}_r)$	Unit base vectors in a helical reference system
$\underline{F}$	Induction factor
$G(x_R)$	Non-dimensional circulation
$i_T(x_R)$	Total rake: axial displacement of blade-section midchord point from x = 0 plane
$(\underline{i}, \underline{e}_r, \underline{e}_\theta)$	Unit base vectors in a cylindrical polar reference system
$(\underline{i}, \underline{j}, \underline{k})$	Unit base vectors in a Cartesian reference frame
$J_V = V/nD$	Advance coefficient based on reference speed
$\underline{N}(x_c, x_R)$	Vector normal to blade surface, pointing into fluid
$N_R(x_c, x_R)$	Radial component of $\underline{N}$
$\underline{N}_o(x_c, x_R)$	Normal to blade-reference surface (E = 0 surface)
$\underline{n}$	Unit vector normal to blade surface, pointing into fluid
n	Propeller rotational speed, revolutions per unit time
p	Pressure
$P(x_R)$	Pitch of blade section
Q	Torque absorbed by blades
$\underline{q} = \underline{q}_\infty + \underline{v}$	Velocity vector
$\underline{q}_\infty$	Velocity vector far upstream
R = D/2	Rotor tip radius
r_h	Radius of rotor hub
$\underline{r}$	Position vector of field point
$\underline{r}_o$	Position vector of field point on blade reference surface
$\underline{s}_b(x_c, x_R)$	Position vector of point on b^{th} blade surface
$\underline{s}_o(x_c, x_R)$	Position vector of point on blade reference surface $\theta_b = 0$
$\underline{s}_{W_b}(\eta, x_R)$	Position vector of point on shed vortex sheet
T	Thrust produced by blades
t	Thickness of blade section
V	Reference speed
$\underline{v}$	Velocity component due to presence of the blades
$\bar{\underline{v}} = (u, v, w)$	Average perturbation velocity along blade surface, due to presence of the blades
$<\underline{v}> = (\gamma, \mu, \sigma)$	Velocity difference across blade surface
$\bar{\underline{v}}_L$	Even perturbation velocity component due to blade loading and shed vortex sheet

$\underline{v}_T$	Even perturbation velocity component due to thickness
$\underline{W}$	Velocity induced by vortex filament
$w_x(x_R)$	Local wake fraction
$w_R(x_R)$	Radial free stream velocity component, fraction of V
(x, y, z)	Cartesian coordinates
x_o	Cartesian coordinate for field point on blade surface
x_c	Fraction of chord, measured from leading edge
x_{c_o}	Fraction of chord for field point on blade surface
x_h	Hub radius, fraction of tip radius
x_R	Fraction of radius, measured from axis of rotation
x_{R_o}	Radial coordinate for field point on blade surface
$Y_T(x_c)$	Nondimensional thickness offset; maximum $Y_T = 0.5$
Z	Number of blades
α	Angular variable in chordwise direction
$\alpha(x_c, x_R)$	Component of derivative of surface coordinate
$\beta = \tan^{-1}\frac{J(1-w_x)}{x_R \pi}$	Advance angle of blade section
$\Gamma(x_R)$	Circulation distribution
$\gamma(x_c, x_R)$	Chordwise component of disturbance velocity difference across blade section
$\gamma^*(x_c)$	Chordwise velocity difference scaled to give unit magnitude when integrated across the chord
ϵ	Error bound; Increment to pitch angle when radial inflow exists
η	Integration variable along vortex filament
$\theta = \tan^{-1}\frac{-y}{z}$	Angular coordinate in cylindrical reference frame
$\theta_b = 2\pi(b-1)/Z$	Angular coordinate of blade-reference line of b^{th} blade
$\theta_s(x_R)$	Skew angle; circumferential displacement of blade-section mid-chord point from y = 0 plane
$\theta_o(x_c, x_R)$	Angular coordinate of point on blade-reference surface
$\underline{\Lambda} = (\sigma, \gamma)$	Vorticity vector
$\mu(x_c, x_R)$	Normal component of disturbance velocity difference across blade section (source strength due to thickness)
(ξ_1, ξ_2, r)	Helical coordinates on pitch reference surface
ρ	Fluid density
$\sigma(x_c, x_R)$	Component of disturbance velocity difference across blade section
σ_s	Surface area
ϕ	Potential function for perturbation velocity; polar coordinate for field point
$\phi_P(x_R) = \tan^{-1}\frac{(P/D)}{\pi x_R}$	Pitch angle of blade reference surface; measured on cylinder of radius r
$\phi_g(x_R)$	Geometric pitch angle
$\psi(x_c)$	Radius of streamline on blade surface
ω	Angular variable in radial direction

INTRODUCTION

The design of an open marine propulsor is a complex process, involving structural and hydrodynamic considerations (1, 2). For the hydrodynamic considerations during most of the preliminary design process, approximate models of the lifting surfaces are employed, e.g., the lifting-line model (3, 4) for powering considerations, and two-dimensional flow over equivalent blade sections for cavitation performance. More sophisticated models of the lifting surfaces are used for predicting fluctuating loads (5) and some cavitation predictions (6). These approximate models have been acceptable during the preliminary design process and provide a basis for choice of the maximum diameter, advance coefficient and radial variations of chord, skew-angle, rake, thickness, and circulation distribution. The chordwise variation in load has usually been selected during this preliminary stage and is often based on cavitation and propulsion considerations.

For the final stage of the design, the meanline distribution and radial pitch variation are determined corresponding to the selections for load and geometry already available. To derive a geometry which accurately produces the specified load distributions, a lifting-surface model of the blades is required.

Several procedures already exist for performing lifting-surface calculations for wide-bladed open marine propulsors. In particular, two different approaches to the analysis for blades with arbitrary locations in space have been presented by Kerwin (7) and McMahon (8). Kerwin's numerical analysis procedure is based on three fundamental assumptions: (1) that the continuous loading distribution on the nonplanar blade surface can be adequately approximated by a multitude of discrete straight lines of constant-vortex strength and that the source distribution arising from the thickness distribution can be similarly approximated, (2) that the minimum required spacing between lattice elements along the chordline is $\Delta\theta = 2$ degrees, and (3) that the resulting meanline shape for a given chordwise load is similar to the two-dimensional shape for the same chordwise load. The first two assumptions are not acceptable for very narrow blades: for a blade with a 20 degree pitch angle at the 0.9

radius and a chord to diameter ratio of 0.05, the 2 degree spacing equals increments of about 1/3 chord length. The last assumption permits calculations to be performed using only a few points along the chord and the two-dimensional shape is fitted to the data at these points. The resulting computer code is relatively quick running and produces a geometry which, in practice, has an overall speed and powering performance generally within a few percent or so of the predicted values, with a general tendency to produce a greater thrust than predicted. The procedure of McMahon employs continuous distributions for the loading and thickness functions and calculates the meanline from the induced velocity. Consequently, data at more chordwise points are required to define the pitch and meanline distributions. The resulting computer code is lengthy to run but has shown remarkably different meanline shapes from the two-dimensional one at the hub and tip region of the blade where the meanlines can be s-shaped (8). Two models were constructed and experimentally evaluated to provide data on the relative cavitation and propulsion performance of designs having the same input specifications but final geometry according to the Kerwin and McMahon procedures. Some inconsistencies occurred in the experimental measurements but the thrust was closer to the predicted value and the operating point centered in the cavitation bucket for the model designed by the McMahon method. Hence, the determination of specific meanline and pitch distributions, instead of fitting the two-dimensional meanline, is considered to be a superior procedure when the design is based on a narrow range of permissible operating conditions and the delay of cavitation is critical.

Because the numerical-analysis procedure employed by McMahon results in lengthy computer runs and Kerwin's procedure is not acceptable for narrow blades, alternative numerical-analysis schemes are investigated in this paper. In addition, a detailed description of the flow field across the blade surface was desired as input into boundary-layer calculations. Two different numerical analysis schemes are described, each involving an expansion of the singular kernel about the singular point. Both approaches employ integration of the specified thickness slope and load distribution over the reference blade in the radial direction first and the remaining chordwise integration then takes the form of the velocity component corresponding to two-dimensional flow modified by the presence of an induction factor in the integral. Regular integration techniques are employed for the other blades and the shed vortex sheet. The induced velocity components are appropriately combined and integrated to obtain meanline shapes.

The present investigation describes the real-fluid flow about a rotating system of lifting surfaces having both loading and thickness. Several approximations are made. The first of these is the mathematical model for which potential flow equations are employed and the solution to first-order in thickness-to-chord ratio, camber-to-chord ratio and difference in pitch and flow angles derived. Comparisons with experimental results for other lifting-surface configurations lead to confidence in this linearized approximation. In addition to this mathematical model, further approximations occur in the numerical analysis. Confidence in the numerical analysis procedures is justified by comparison with analytical solutions or experimental results. That is, results are sought from some discretized numerical-analysis procedures involving N by M approximations, which have converged to within some specified tolerance, ϵ, of the real or analytical value of the quantity investigated. Mathematically this may be stated

$$| f(x, y) - f_{N,M}(x, y) | \leq \epsilon$$

$$\text{for} \begin{cases} (x, y) \text{ on the surface } S \\ N \geq N_o \\ M \geq M_o \end{cases}$$

where $f_{N,M}$ = the approximate calculation of a particular quantity f

S = a region of the surface of interest

N_o, M_o = minimum numbers of the discrete approximations for which the computed results are within ϵ of the values for f

For rotating lifting surfaces, neither measured nor analytical solutions exist for details of the flow field on the blade. Hence, comparisons will be made with other procedures. It is assumed that numerical solutions which employ increasingly greater pointwise definition of the input variable without change in computed values have converged and that the solution has converged when a smooth curve can be drawn through point values in both the chordwise and radial directions. These assumptions are believed to be necessary but not sufficient for convergence.

In the following sections, the mathematical model of the flow field on the blade surface is first reviewed and numerical-analysis techniques for evaluating both regular and singular integrals are described. A FORTRAN computer code is discussed and sample calculations using this code are presented. From example calculations, it is found that greater accuracy in the integral evaluations is required for the determination of smooth pressure distribution curves than for the shape of the meanline and the pitch distributions. The choice of a particular chordwise loading distribution is shown to have an effect on the meanline shape and the pressure distribution. The effects of rake and skew are shown to be important on both pressure distribution and meanline shape. A particular thickness function has hardly any effect on pitch or meanline but a significant effect on pressure distribution.

MATHEMATICAL MODEL – THICK LIFTING BLADE

The mathematical model of a system of rotating lifting surfaces advancing in an unbounded irrotational flow field with an inviscid fluid has been developed on a formal mathematical basis by Brockett (9). A reformulation of that analysis in terms of non-dimensional surface coordinates is presented herein for completeness. The propulsor is assumed to be adequately represented by the blades alone, i.e., neither the hub nor fillet from the blades to the hub is included in the blade specification. The onset flow is assumed to be directed along the axis of rotation but a new feature included herein is that it may have a small radial component. Overall geometry notation generally follows the definitions given in Reference 10.

Coordinate systems are constructed with the same orientation as in Reference 9, and in particular, the helical coordinate system (ξ_1, ξ_2, r) rotating with the blades is shown in Figure 1. Unit base vectors in a right-handed Cartesian reference frame are the customary ($\underline{i}$, $\underline{j}$, $\underline{k}$) where $\underline{i}$ is along the x axis and is positive pointing aft, $\underline{j}$ is along the y axis and $\underline{k}$ is along the z axis which is generally along the reference blade. Unit vectors along the helical coordinates are

$$\underline{e}_1 = \sin \phi_P \, \underline{i} + \cos \phi_P \, \underline{e}_\theta \tag{1}$$

$$\underline{e}_2 = -\cos \phi_P \, \underline{i} + \sin \phi_P \, \underline{e}_\theta \tag{2}$$

$$\underline{e}_r = -\sin \theta \, \underline{j} + \cos \theta \, \underline{k} \tag{3}$$

where

$$\underline{e}_\theta = -\cos \theta \, \underline{j} - \sin \theta \, \underline{k} \tag{4}$$

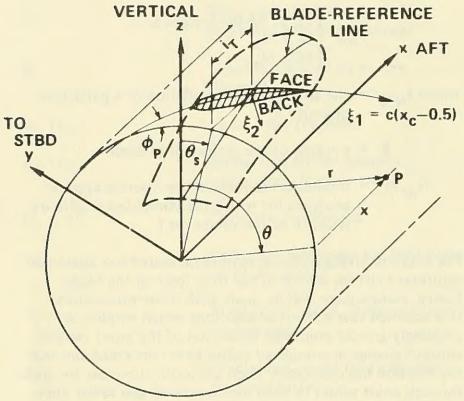

Fig. 1 Lifting-surface geometry

The blade surface is given by

$$\xi_2 = E(\xi_1, r) \tag{5}$$

$$= E_c(\xi_1, r) \pm E_T(\xi_1, r) \tag{6}$$

where

E_c is the meanline shape, and

E_T is the thickness shape

In the analysis, it is convenient to change the variables of integration to (x_c, x_R) instead of (ξ_1, r), where

$$\left.\begin{aligned} \xi_1 &= c\,(x_c - 0.5) \\ r &= D\,x_R/2 \\ c &= \text{chordlength at radius } r \\ \text{and} \\ D &= \text{maximum rotor diameter} \end{aligned}\right\} \tag{7}$$

The position vector of a point on the blade surface described by Equation (5) is

$$\underline{s} = D\left\{\left[\frac{i_T}{D} + \frac{c}{D}(x_c - 0.5)\sin\phi_P - \frac{E}{D}\cos\phi_P\right]\underline{i} + \frac{x_R}{2}\,\underline{e}_r(\theta)\right\} \tag{8}$$

and a normal, directed out from the blade surface, is (9, 11)

$$\underline{N} = \pm\,\frac{\partial \underline{s}}{\partial x_c} \times \frac{\partial \underline{s}}{\partial x_R} \tag{9}$$

where the plus sign is used for the suction side of the blade and the negative sign for the pressure side of the blade. After some effort it can be shown that

$$\underline{N} = \pm\,\frac{D^2}{2}\left\{\frac{c}{D}\,\underline{e}_2 - \frac{\partial E/D}{\partial x_c}\,\underline{e}_1 + N_R\,\underline{e}_r\right\} \tag{10}$$

where

$$\begin{aligned} N_R = &-2\,\frac{c}{D}\,\frac{\partial E/D}{\partial x_R} + 2\,(x_c - 0.5)\,\frac{d\,c/D}{d\,x_R}\,\frac{\partial E/D}{\partial x_c} \\ &+ 2\,\frac{d\,i_T/D}{d\,x_R}\left[\frac{c}{D}\cos\phi_P + \frac{\partial E/D}{\partial x_c}\sin\phi_P\right] \\ &+ 2\left[\left(\frac{c}{D}\right)^2 (x_c - 0.5) + \frac{E}{D}\,\frac{\partial E/D}{\partial x_c}\right] \\ &\cdot\left[\frac{d\,P/D}{d\,x_R}\,\frac{\cos^2\phi_P}{\pi\,x_R} - \frac{\sin\phi_P\cos\phi_P}{x_R}\right] \\ &-\left[x_R\,\frac{d\,\theta_s}{d\,x_R} - 2\,\frac{\frac{c}{D}(x_c - 0.5)\cos\phi_P + \frac{E}{D}\sin\phi_P}{x_R}\right] \\ &\cdot\left[\frac{c}{D}\sin\phi_P - \frac{\partial E/D}{\partial x_c}\cos\phi_P\right] \end{aligned}$$

The normal to the blade reference surface, $\xi_2 = 0$, $0 \le x_c \le 1$, $x_h \le x_R \le 1$ is

$$\underline{N}_o = \pm\,\frac{D^2}{2}\,\frac{c}{D}\left[\underline{e}_2 + N_{R_o}\,\underline{e}_r(\theta_o)\right] \tag{11}$$

where

$$N_{R_o} = 2\,\frac{d\,i_T/D}{d\,x_R}\cos\phi_P + 2\left(\frac{c}{D}\right)(x_c - 0.5) \cdot \frac{d\,P/D}{d\,x_R}\,\frac{\cos^2\phi_P}{\pi\,x_R} - x_R\,\frac{d\,\theta_s}{d\,x_R}\sin\phi_P$$

N_{R_o}, the radial component of the normal, is zero for a constant-pitch blade which is neither raked nor skewed. In Equations (10) and (11):

i_T = the total rake

P = the pitch of the blade

ϕ_P = the pitch angle, $\phi_P = \tan^{-1}(P/(\pi x_R D))$

θ = the angular position of a point on the blade surface, a function of both x_c and x_R

$$= 2\,\frac{b-1}{Z}\,\pi + \theta_s + 2\left[\frac{c}{D}(x_c - 0.5)\cos\phi_P + \frac{E}{D}\sin\phi_P\right]\Big/ x_R$$

θ_s = the skew angle, a function of x_R

and

$$\theta_o = 2\,\frac{b-1}{Z}\,\pi + \theta_s + 2\,\frac{c}{D}\,(x_c - 0.5)\cos\phi_P / x_R$$

In the derivation of the expressions for numerical analysis, the reference surface (E = 0) is often employed. Generally no specific mention will be made of differences between variables on the blade surface and on the reference surface.

In a coordinate system rotating with the blades, the fluid velocity may be taken to be the sum of the undisturbed velocity and a component due to the disturbance of the blades:

$$\underline{q} = V(1 - w_x(x_R))\ \underline{i} + 2\pi n\ r\ \underline{e}_\theta + V w_R(x_R)\ \underline{e}_r + \underline{v} \tag{12}$$

$$= \underline{q}_\infty + \underline{v} \tag{13}$$

where V = the constant reference speed

$1-w_x$ = the wake-fraction multiple to obtain the local axisymmetric speed[1]

w_R = the radial component of inflow, fraction of the reference speed

n = the rotational speed, revolutions per unit time, and

$\underline{v}$ = the velocity component due to the presence of the blades

If ϕ_P is the pitch angle and β is the advance angle

$(\beta = \tan^{-1}\{V(1-w_x)/(2\pi n r)\})$

then

$$\frac{q_\infty}{V} = \sqrt{(1-w_x)^2 + \left(\frac{\pi x_R}{J_v}\right)^2} \cdot \left\{\cos(\phi_P - \beta)\ \underline{e}_1 + \sin(\phi_P - \beta)\ \underline{e}_2\right\} + w_R\ \underline{e}_r \tag{14}$$

where the advance coefficient, J_v, is given by

$$J_v = V/(nD) \tag{15}$$

The boundary condition on the blade is that there be no flow through the surface:

$$\underline{q} \cdot \underline{N} = 0 \text{ for } \underline{r} \text{ on } S \tag{16}$$

This condition applies to both the upper and lower surfaces:

$$\underline{q}^+ \cdot \underline{N}^+ = 0 \tag{17}$$

$$\underline{q}^- \cdot \underline{N}^- = 0 \tag{18}$$

The sum of Equations (17) and (18) is:

$$\underline{q} \cdot (\underline{N}^+ + \underline{N}^-) + \underline{v}^+ \cdot \underline{N}^+ + \underline{v}^- \cdot \underline{N}^- = 0$$

Now

$$\underline{q}_\infty \cdot (\underline{N}^+ + \underline{N}^-) = -D^2 \frac{\partial E_T/D}{\partial x_c}(\underline{q}_\infty \cdot \underline{e}_1) + 0(E, w_R) \tag{19}$$

thus to first order in w_R or E:

$$\underline{v}^+ \cdot \underline{N}^+ + \underline{v}^- \cdot \underline{N}^- = D^2 V \sqrt{(1-w_x)^2 + \left(\frac{\pi x_R}{J_v}\right)^2} \cdot \cos(\phi_P - \beta) \frac{\partial (E_T/D)}{\partial x_c} \approx \underline{N}_o^+ \cdot (\underline{v}^+ - \underline{v}^-) \tag{20}$$

[1] As described in Reference 9, the inclusion of a radially variable inflow introduces vorticity into the mathematical model. No specific consideration is undertaken to account for this vorticity.

The difference of Equations (17) and (18) gives:

$$\underline{v}^+ \cdot \underline{N}^+ - \underline{v}^- \cdot \underline{N}^- = -\underline{q}_\infty \cdot (\underline{N}^+ - \underline{N}^-)$$

$$= -\underline{q}_\infty \cdot \left[2\,\underline{N}_o^+ - D^2 \frac{\partial \frac{E_c}{D}}{\partial x_c}\underline{e}_1 + 0(E)\,\underline{e}_r\right]$$

$$= -\left(2\,\underline{q}_\infty \cdot \underline{N}_o^+ - D^2 \frac{\partial \frac{E_c}{D}}{\partial x_c}\underline{q}_\infty \cdot \underline{e}_1\right) + 0(E, w_R)$$

$$= -D^2 V \left[\sqrt{(1-w_x)^2 + \left(\frac{\pi x_R}{J_v}\right)^2} \cdot \left(\frac{c}{D}\sin(\phi_P - \beta) - \frac{\partial E_c/D}{\partial x_c}\cos(\phi_P - \beta)\right) + \frac{c}{D} w_R N_{R_o}\right] + 0(E, w_R) \tag{21}$$

$$\approx \underline{N}_o^+ \cdot (\underline{v}^+ - \underline{v}^-)$$

or

$$\frac{\partial \frac{E_c}{D}}{\partial x_c} = \frac{c}{D}\left[\tan(\phi_P - \beta) + \frac{\underline{N}_o^+ \cdot (\underline{v}^+ + \underline{v}^-)/(D^2 V\, c/D) + w_R N_{R_o}}{\cos(\phi_P - \beta)\sqrt{(1-w_x)^2 + \left(\frac{\pi x_R}{J_v}\right)^2}}\right] \tag{22}$$

This is the fundamental equation to be evaluated to determine the pitch and meanline shape. The slope of the meanline is given as a function of known geometry and inflow quantities plus the normal component of the average induced velocity on the blade surface. Hence to determine the meanline slope, the mean perturbation velocity must be determined on the blade surface.

The velocity component due to the disturbance of the blades, $\underline{v}$, can be shown to be potential in nature (9). Hence, it can be represented by an equation (9, 12)

$$\underline{v}(\underline{r}) = \frac{1}{4\pi}\sum_{b=1}^{Z}\iint_S \left[\underline{n} \cdot \underline{v}\frac{\underline{r} - \underline{s}_b}{|\underline{r} - \underline{s}_b|^3} + (\underline{n} \times \underline{v}) \times \frac{\underline{r} - \underline{s}_b}{|\underline{r} - \underline{s}_b|^3}\right] d\sigma_s \tag{23}$$

where $\underline{n}$ is a unit normal pointing into the fluid from a point $\underline{s}$ on the surface S (including both the blades and shed vortex sheet), and $d\sigma_s$ is the area element.

In several texts (11, 12), it is shown that

$$\underline{n}\, d\sigma_s = \underline{N}\, dx_c\, dx_R \tag{24}$$

In Equation (23), it is convenient to let the region of integration be the blade reference surface $\xi_2 = 0$, $0 \le x_c \le 1$, $x_h \le x_R \le 1$, for which

$$\underline{s}_b \equiv \underline{s}_{o_b} = D\left\{\left[\frac{i_T}{D} + \frac{c}{D}(x_c - 0.5)\sin\phi_P\right]\underline{i} + \frac{x_R}{2}\underline{e}_r(\theta_o)\right\} \quad (25)$$

Hence, Equation (23) can be reduced to an integral over only one side of the blade surfaces and shed vortex sheets:

$$\underline{v}(\underline{r}) = \frac{1}{4\pi}\sum_{b=1}^{Z}\int_0^1 d\,x_c \int_{x_h}^1 d\,x_R \cdot \left[(\underline{N}^+ \cdot \underline{v}^+ + \underline{N}^- \cdot \underline{v}^-)\frac{\underline{r}-\underline{s}_{o_b}}{\left|\underline{r}-\underline{s}_{o_b}\right|^3} + (\underline{N}^+ \times \underline{v}^+ + \underline{N}^- \times \underline{v}^-)\times\frac{\underline{r}-\underline{s}_{o_b}}{\left|\underline{r}-\underline{s}_{o_b}\right|^3}\right] + \frac{1}{4\pi}\sum_{b=1}^{Z}\int_{x_h}^1 dx_R \int_0^\infty d\eta\,\frac{dx_c}{d\eta}[\underline{N}^+ \times (\underline{v}^+ - \underline{v}^-)] \times \frac{\underline{r}-\underline{s}_{w_b}}{\left|\underline{r}-\underline{s}_{w_b}\right|^3} \quad (26)$$

where:

$$\frac{\underline{s}_{w_b}}{D} = \left(\frac{x_{te}}{D} + \eta\sin\phi_P\right)\underline{i} + \frac{x_R}{2}\underline{e}_r(\theta_{te} + 2\eta\cos\phi_P/x_R + \theta_b)$$

and

$$\eta = \frac{c}{D}(x_c - 1.0)$$

As the field point $\underline{r}$ approaches a point $\underline{r}_o(x_{c_o}, x_{R_o})$ on the surface of the blade, Equation (23) or (26) becomes singular. If a small region about this point is excluded from the surface S and the limit of the integral taken for $\underline{r} \to \underline{r}_o$ with the excluded area tending to zero, there results (see Reference 9):

$$\lim_{\underline{r}\to\underline{r}_o^+}[\underline{v}(\underline{r})] = \frac{1}{4\pi}\sum_{b=1}^{Z}\oint_0^1 dx_c \oint_{x_h}^1 dx_R \cdot \left[(\underline{N}^+ \cdot \underline{v}^+ + \underline{N}^- \cdot \underline{v}^-)\frac{\underline{r}_o-\underline{s}_{o_b}}{\left|\underline{r}_o-\underline{s}_{o_b}\right|^3} + (\underline{N}^+ \times \underline{v}^+ + \underline{N}^- \times \underline{v}^-)\times\frac{\underline{r}_o-\underline{s}_{o_b}}{\left|\underline{r}_o-\underline{s}_{o_b}\right|^3}\right] + \frac{1}{2}[\underline{v}^+(\underline{r}_o) - \underline{v}^-(\underline{r}_o)] \quad (27)$$

$$+ \frac{1}{4\pi}\sum_{b=1}^{Z}\int_{x_h}^1 dx_R \int_0^\infty d\eta\,\frac{dx_c}{d\eta} \cdot \frac{[\underline{N}^+ \times (\underline{v}^+ - \underline{v}^-)] \times (\underline{r} - \underline{s}_{w_b})}{\left|\underline{r}_o - \underline{s}_{w_b}\right|^3} \quad (27\ \text{cont.})$$

where the symbol $\oint$ means symmetry restrictions occur for the limiting region which excludes the singularity. For example (9), the region may be square, circular, or rectangular centered at $\underline{r}_o$. In the present application, the rectangular region $x_{c_o} - \epsilon \le x_c \le x_{c_o} + \epsilon$, $x_h \le x_R \le 1$ will be the shape of the excluded region. Then this principal value integral is defined

$$\oint_0^1 dx_c \int_{x_h}^1 dx_R\ \underline{K} = \lim_{\epsilon\to 0}\left[\int_0^{x_{c_o}-\epsilon} dx_c \int_{x_h}^1 dx_R\ \underline{K} + \int_{x_{c_o}+\epsilon}^1 dx_c \int_{x_h}^1 dx_R\ \underline{K}\right] \quad (28)$$

The assumption

$$\lim_{\underline{r}\to\underline{r}_o^+}[\underline{v}(\underline{r})] = \underline{v}^+(\underline{r}_o) \quad (29)$$

(i.e., that the velocity defined in the field does approach the value on the boundary) leads to the following expression for the average velocity component on the blade surface

$$\overline{\underline{v}}\left(x_{c_o}, x_{R_o}\right) \equiv \frac{1}{2}\left[\underline{v}^+\left(x_{c_o}, x_{R_o}\right) + \underline{v}^-\left(x_{c_o}, x_{R_o}\right)\right] \quad (30)$$

$$= \overline{\underline{v}}_L + \overline{\underline{v}}_T$$

$$= u\underline{e}_1 + v\underline{e}_2 + w\underline{e}_r$$

$$= \sum_{b=1}^{Z}\oint_0^1 dx_c \int_{x_h}^1 dx_R\ \underline{K}\left(x_{c_o}, x_{R_o}, x_c, x_R\right) + \underline{v}_w \quad (31)$$

where the singular kernel is

$$\underline{K}\left(x_{c_o}, x_{R_o}, x_c, x_R\right) = \frac{1}{4\pi}\left[(\underline{N}^+ \cdot \underline{v}^+ + \underline{N}^- \cdot \underline{v}^-) \cdot \frac{\underline{r}_o - \underline{s}_{o_b}}{\left|\underline{r}_o - \underline{s}_{o_b}\right|^3} + (\underline{N}^+ \times \underline{v}^+ + \underline{N}^- \times v^-) \times \frac{\underline{r}_o - \underline{s}_{o_b}}{\left|\underline{r}_o - \underline{s}_{o_b}\right|^3}\right]$$

and the velocity induced by the shed vortex sheet is

$$\underline{v}_w = \frac{1}{4\pi} \sum_{b=1}^{Z} \int_{x_h}^{1} dx_R \int_0^{\infty} d\eta \frac{dx_c}{d\eta} \cdot \frac{[\underline{N}^+ \times (\underline{v}^+ - \underline{v}^-)] \times (\underline{r}_o - \underline{s}_{w_b})}{\left|\underline{r}_o - \underline{s}_{w_b}\right|^3}$$

The first term in Equation (27), the strength of the sources, is known from Equation (20). The strength of the vortex component:

$$\underline{N}^+ \times \underline{v}^+ + \underline{N}^- \times \underline{v}^- \approx \underline{N}_o^+ \times (\underline{v}^+ - \underline{v}^-) \qquad (32)$$

has yet to be determined both on the blades and along the shed vortex sheet. To find a value for this term, it is appropriate to look at the condition that the blade section develop a force at a given radial station

$$\underline{F}(x_R) = -\oint p\, \underline{n}\, d\ell \qquad (33)$$

To first order the local lift is

$$L = \underline{F} \cdot \underline{e}_2 = D \frac{c}{D} \int_0^1 (p^- - p^+)\, d x_c \qquad (34)$$

Bernoulli's equation can be constructed for a coordinate system rotating with the blade (9) and the pressure difference determined by

$$p^- - p^+ = \frac{\rho}{2}\left\{(q^+)^2 - (q^-)^2\right\} \qquad (35)$$

$$= \rho\left\{\underline{q}_\infty \cdot (\underline{v}^+ - \underline{v}^-) + \frac{1}{2}(\underline{v}^+ + \underline{v}^-) \cdot (\underline{v}^+ - \underline{v}^-)\right\}$$

$$\approx \rho\, \underline{q}_\infty \cdot (\underline{v}^+ - \underline{v}^-) \qquad (36)$$

Let

$$\langle \underline{v} \rangle \equiv \frac{1}{2}[\underline{v}^+ - \underline{v}^-] = \frac{\gamma}{2}\underline{e}_1 + \frac{\mu}{2}\frac{\underline{N}_o^+}{|\underline{N}_o^+|^2} + \frac{\sigma}{2}\pi D^2 V \frac{\underline{N}_o^+ \times \underline{e}_1}{|\underline{N}_o^+|^2} \qquad (37)$$

Then to first order

$$\gamma = \frac{p^- - p^+}{\rho V \sqrt{(1 - w_x)^2 + \left(\frac{\pi x_R}{J_v}\right)^2} \cos(\phi_P - \beta)} \qquad (38)$$

$$= \frac{V}{2} \frac{\Delta C_p}{\sqrt{(1 - w_x)^2 + \left(\frac{\pi x_R}{J_v}\right)^2} \cos(\phi_P - \beta)} \qquad (39)$$

and from Equation (20):

$$\mu = D^2 V \sqrt{(1 - w_x)^2 + \left(\frac{\pi x_R}{J_v}\right)^2} \cos(\phi_P - \beta) \frac{\partial E_T/D}{\partial x_c} \qquad (40)$$

where:

$$\Delta C_p = (p^- - p^+) / (\rho V^2/2) \qquad (41)$$

It remains to determine σ. Now, in general

$$\underline{N}_o^+ \times (\underline{v}^+ - \underline{v}^-) = -\pi D^2 V \sigma \underline{e}_1 + \gamma (\underline{N}_o^+ \times \underline{e}_1) \qquad (42)$$

and the value of σ can be determined by setting the divergence of the right-hand-side equal to zero (9). However, this results in a differential equation to be solved for σ. A more direct procedure is to express the perturbation velocity vector as the gradient of a potential:

$$\underline{v} = \nabla\phi \qquad (43)$$

where

$$\phi(\underline{r}) = \lim_{A \to \infty} \int_{-A\underline{i}}^{\underline{r}} \underline{v} \cdot d\underline{\ell} \qquad (44)$$

Thus

$$\langle \underline{v} \rangle \equiv \frac{1}{2}[\underline{v}^+ - \underline{v}^-] = \frac{1}{2}\lim_{\substack{\underline{r} \to \underline{r}_o^+ \\ A \to \infty}} \left[\nabla \int_{-A\underline{i}}^{\underline{r}} \underline{v} \cdot d\underline{\ell}\right] - \frac{1}{2}\lim_{\substack{\underline{r} \to \underline{r}_o^- \\ A \to \infty}} \left[\nabla \int_{-A\underline{i}}^{\underline{r}} \underline{v} \cdot d\underline{\ell}\right] \qquad (45)$$

and

$$\frac{\underline{N}_o^+ \times \langle \underline{v} \rangle}{2\pi D^2 V} = \frac{\underline{N}_o^+}{4\pi D^2 V} \times \left[\nabla \int_{le}^{r_o} (\underline{v}^+ - \underline{v}^-) \cdot d\underline{\ell}\right] \qquad (46)$$

For $d\underline{\ell} = D\frac{c}{D}\underline{e}_1\, dx_c$,

$$\frac{\underline{N}_o^+ \times \langle \underline{v} \rangle}{2\pi D^2 V} = \frac{\underline{N}_o^+}{4\pi D^2 V} \times \nabla \left[D\frac{c}{D}\int_o^{x_c} \gamma\, dx_c\right] \qquad (47)$$

It is convenient to define

$$\gamma(x_c, x_R) = \frac{1}{D} \frac{\Gamma(x_R)\, \gamma^*(x_c)}{c/D} \qquad (48)$$

where $\Gamma(x_R)$ is the bound circulation ($\phi^+ - \phi^-$ at the trailing edge and points beyond), and γ^* has unit magnitude when integrated across the chord. Let the nondimensional circulation G be

$$G = \frac{\Gamma}{\pi D V} \qquad (49)$$

Then

$$\gamma = \pi V \frac{G(x_R)\, \gamma^*(x_c)}{c/D} \qquad (50)$$

and

$$\underline{\Lambda} \equiv \frac{\underline{N}_o^+ \times \langle \underline{v} \rangle}{2\pi D^2 V} = \frac{\underline{N}_o^+}{4\pi D^2 V} \times \nabla \left[\pi V D G(x_R) \int_o^{x_c} \gamma^*\, dx_c\right] \qquad (51)$$

$$= \frac{\underline{N}_o^+}{4D} \times \nabla \left[G(x_R) \int_o^{x_c} \gamma^* \, dx_c \right] \tag{52}$$

In Reference 9, the gradient of a scalar function is derived for a general helical coordinate system. From this expression one obtains:

$$\underline{\Lambda} = \frac{\underline{N}_o^+}{4D^2 \frac{c}{D}} \times \left[G\gamma^* \, \underline{e}_1 + 2\left(\frac{c}{D} \frac{dG}{dx_R} \int_o^{x_c} \gamma^* \, dx_c - \alpha G \gamma^* \right) \underline{e}_r \right] \tag{53}$$

$$= -\frac{1}{4}\left(\frac{c}{D} \frac{dG}{dx_R} \int_o^{x_c} \gamma^* \, dx_c - \alpha G \gamma^* \right) \underline{e}_1 + \frac{1}{8} G\gamma^* \frac{\underline{N}_o^+ \times \underline{e}_1}{\frac{D^2}{2} \frac{c}{D}} \tag{54}$$

Hence from Equation (40):

$$\sigma = \frac{c}{D} \frac{dG}{dx_R} \int_o^{x_c} \gamma^* \, dx_c - \alpha G \gamma^* \tag{55}$$

where

$$\alpha = \left(\frac{d \frac{c}{D}}{dx_R} - \frac{c}{D} \frac{\cos^2 \phi_P}{x_R} \right) (x_c - 0.5) + \frac{x_R}{2} \cos \phi_P \frac{d\theta_s}{dx_R} + \sin \phi_P \frac{d \frac{i_T}{D}}{dx_R} \tag{56}$$

At the trailing edge and beyond

$$\gamma^* (1) = 0 \tag{57}$$

$$\int_o^1 \gamma^* \, dx_c = 1 \tag{58}$$

Hence

$$\underline{\Lambda} = -\frac{1}{4} \frac{c}{D} \frac{dG}{dx_R} \underline{e}_1 \tag{59}$$

for the shed vortex wake.

Thus, the strength of the vortex distribution is explicitly known and the integration to determine the average induced velocity at points on the blade surface can be undertaken.

Once the induced velocity field on the blade is computed, the meanline slope can be determined and the meanline offset can be found by integrating the slope:

$$\frac{E_c (x_{c_o}, x_R)}{D} = \int_o^{x_{c_o}} \frac{\partial \frac{E_c (x_c, x_R)}{D}}{\partial x_c} \, dx_c \tag{60}$$

From Equation (22), the meanline offset for the term with the radial inflow velocity component can be directly computed; it consists of an angle of attack term due to gradient of the rake and skew terms and a parabolic arc meanline due to gradients of the pitch.

In general, the trailing edge point will not be zero. The trailing-edge offset can be converted into a pitch-angle increment,

$$\tan (\phi_g - \phi_P) = -E_c (1, x_R)/c \tag{61}$$

$$\phi_g = \phi_P + \tan^{-1} \left[\frac{E_c (1, x_R)}{D} \Big/ \left(\frac{c}{D} \right) \right] \tag{62}$$

for which the pitch of the nose-tail line becomes

$$\left. \frac{P}{D} \right|_{nt} = \pi x_R \tan \phi_g = \frac{\pi x_R \tan \phi_P + \pi x_R (-E_c (1, x_R)/c)}{1 - \tan \phi_P (-E_c (1, x_R)/c)} \tag{63}$$

and meanline ordinates measured from the nose-tail line can be determined:

$$\left. \frac{E_c}{D} \right|_{nt} = \frac{E_c}{D} - \frac{E_c (1, x_R)}{D} \, x_c \tag{64}$$

These values of corrected pitch and meanline shapes relative to the nose-tail line are the essential data produced by the lifting-surface analysis.

In addition to the meanline and pitch distributions, several other quantities of interest can be computed. These are pressure distribution, total forces, and streamline coordinates (this coordinate system is described in the Appendix).

From Reference 9, the pressure coefficient is

$$C_p = \frac{p - p_\infty}{\frac{1}{2} \rho V^2} \tag{65}$$

$$= \frac{\underline{q}_\infty \cdot \underline{q}_\infty - \underline{q} \cdot \underline{q}}{V^2} \tag{66}$$

An approximation for the non-linear speed on the surface of the blade in the chordwise direction is (13)

$$\frac{q_s}{V} \doteq \frac{\sqrt{(1 - w_x)^2 + \left(\frac{\pi x_R}{J_v} \right)^2} + \underline{v} \cdot \underline{e}_1}{\sqrt{1 + \left(\frac{\partial (E_T / c)}{\partial x_c} \right)^2}} \tag{67}$$

Hence

$$\left(\frac{q}{V} \right)^2 = \left(\frac{q_s}{V} \right)^2 + \left(w_R \, \underline{e}_r \cdot \hat{\underline{e}} + \frac{\underline{v}}{V} \cdot \hat{\underline{e}} \right)^2 \tag{68}$$

where $\hat{\underline{e}}$ is the unit vector in the $\underline{N}_o^+ \times \underline{e}_1$ direction (nearly the radial direction over much of the blade):

$$\hat{\underline{e}} \equiv \frac{\underline{N}_o^+ \times \underline{e}_1}{|\underline{N}_o^+ \times \underline{e}_1|} = \frac{\underline{e}_r - N_{R_o} \underline{e}_2}{\sqrt{1 + N_{R_o}^2}} \tag{69}$$

In Equations (67) and (68), the velocity components $\underline{v} \cdot \underline{e}_1$ and $\underline{v} \cdot \hat{\underline{e}}$ are

$$\frac{\underline{v}}{V} \cdot \underline{e}_1 = \underline{e}_1 \cdot \left(\frac{\bar{\underline{v}}}{V} \pm \frac{<\underline{v}>}{V} \right) = \frac{u}{V} \pm \frac{\gamma}{2V} \tag{70}$$

$$\frac{\underline{v}}{V} \cdot \hat{\underline{e}} = \hat{\underline{e}} \cdot \left(\frac{\bar{\underline{v}}}{V} \pm \frac{<\underline{v}>}{V} \right) = \frac{\frac{w}{V} - \frac{vN_{R_o}}{V} \pm \sigma \frac{\pi}{c/D}}{\sqrt{1 + N_{R_o}^2}} \tag{71}$$

Each of the components $\bar{v}$ and $<\bar{v}>$ has terms due to thickness and terms due to loading.

To first order, the pressure coefficient is

$$C_p = -2 \sqrt{(1 - w_x)^2 + \left(\frac{\pi x_R}{J_v} \right)^2} \left(\frac{u}{V} \pm \frac{\gamma}{2V} \right) \tag{72}$$

Hence the pressure difference to first order is

$$\Delta C_p = C_p^- - C_p^+ = 2 \sqrt{(1 - w_x)^2 + \left(\frac{\pi x_R}{J_v} \right)^2} \frac{\gamma}{V} \tag{73}$$

$$= 2\pi \sqrt{(1 - w_x)^2 + \left(\frac{\pi x_R}{J_v} \right)^2} \, G(x_R) \frac{\gamma^*(x_c)}{c/D} \tag{74}$$

which is independent of rake, skew, or pitch variations (to first order).

Once the pressure distribution on the blade surface is known, the thrust and torque in inviscid flow may be calculated (9). In terms of a thrust and power coefficient, these inviscid overall performance values are:

$$C_{Th_i} = \frac{T_i}{\frac{1}{2}\rho V^2 \pi \frac{D^2}{4}} \tag{75}$$

$$= \frac{2Z}{\pi} \int_{x_h}^{1} dx_R \int_{0}^{1} dx_c \left[\Delta C_p \left(\frac{c}{D} \cos \phi_P + \frac{\partial \frac{E_c}{D}}{\partial x_c} \sin \phi_P \right) - \bar{C}_p \frac{\partial \frac{E_T}{D}}{\partial x_c} \sin \phi_P \right] \tag{76}$$

$$C_{P_i} = \frac{2\pi n Q_i}{\frac{1}{2}\rho V^3 \pi \frac{D^2}{4}} \tag{77}$$

$$= \frac{2Z}{J_v} \int_{x_h}^{1} x_R \, dx_R \int_{0}^{1} dx_c \left[\Delta C_p \left(\frac{c}{D} \sin \phi_P - \frac{\partial \frac{E_c}{D}}{\partial x_c} \cos \phi_P \right) + \bar{C}_p \frac{\partial \frac{E_T}{D}}{\partial x_c} \cos \phi_P \right] \tag{78}$$

where $\Delta C_p = C_p^- - C_p^+$

and $C_p = C_p^- + C_p^+$

The effects of pitch, skew and rake enter into the determination of pressure and are not explicitly in the integrands for thrust and torque.

A correction for viscous drag may be made by assuming the drag force acts along the pitch line. For a given drag coefficient C_D, the force will be approximately

$$D_f = \frac{1}{2}\rho V^2 \left[(1 - w_x)^2 + \left(\frac{\pi x_R}{J_v} \right)^2 \right] \frac{c}{D} \, D C_D \tag{79}$$

When the effects of this force are included in the thrust and power coefficients, one obtains

$$C_{Th} = C_{Th_i} + \Delta C_{Th} \tag{80}$$

$$C_P = C_{P_i} + \Delta C_P \tag{81}$$

where

$$\Delta C_{Th} = -\frac{2Z}{\pi} \int_{x_h}^{1} C_D \left[(1 - w_x)^2 + \left(\frac{\pi x_R}{J_v} \right)^2 \right] \frac{c}{D} \sin \phi_P \, dx_R \tag{82}$$

and

$$\Delta C_P = \frac{2Z}{J} \int_{x_h}^{1} x_R C_D \left[(1 - w_x)^2 + \left(\frac{\pi x_R}{J_v} \right)^2 \right] \frac{c}{D} \cos \phi_P \, dx_R \tag{83}$$

Hence the thrust will be reduced and the torque increased relative to the inviscid values, as expected.

In the Appendix, the formulation for a streamline coordinate system on the blade surface is given.

NUMERICAL ANALYSIS PROCEDURE

The computation of the meanline slope relative to the blade-reference surface (Equation 22) involves some straightforward computations of geometry gradients, which are handled by spline functions, to determine $\underline{N}_o^+$ plus the evaluation of the even velocity component across the blade surface (Equation 30). This even velocity component arises from the odd velocity component (Equation 37) integrated over the blade surfaces and trailing vortex sheets. The magnitude of the odd velocity component is known from Equations (40), (50) and (55). A singularity occurs on the reference blade and special procedures must be employed on that blade. Integration over the other blades can be based on conventional integration procedures. Integration over the infinite shed vortex sheet is truncated to a finite extent. Once the slope is known, it can be integrated across the chord to produce the meanline offset (Equation 60).

For regular integration over the span or chord of the blade, trigonometric polynomials are employed which precisely fit a set of tabulated values given at equal angular increments in α or ω where

$$x_c = \frac{1}{2}(1 - \cos \alpha), \quad 0 \le \alpha \le \pi \tag{84}$$

$$x_R = \frac{1}{2}[1 + x_h - (1 - x_h) \cos \omega], \quad 0 \le \omega \le \pi \tag{85}$$

Details of the curve fitting procedure are contained in Reference 14. Once the trigonometric polynomials are specified, they may be integrated to any point in the closed interval 0 to π. The resulting expressions may be arranged to produce a set of coefficients which are multiples of each tabulated functional value. Then a summation of the coefficients times the tabulated value yields the integral value. A computer code was developed for a subroutine to determine these coefficients for an array of arbitrary values of the independent angular variable between 0 and π when the tabulated values were fit by either a half-range sine or cosine series. The coefficients are stored in the subroutine for repeated use.

For example, the meanline offset is

$$\frac{E_c(\alpha_o, x_R)}{D} = \int_0^{\alpha_o} \left[\frac{\partial \frac{E_c}{D}}{\partial x_c} \frac{\sin\alpha}{2} \right] d\alpha \qquad (86)$$

The slope of the meanline $\frac{\partial \frac{E_c}{D}}{\partial x_c}$ is assumed to be finite at both the leading and trailing edges which results in a sine term approximation for the term in square brackets:

$$\frac{\partial \frac{E_c}{D}}{\partial x_c} \cdot \frac{\sin\alpha}{2} = \sum_{n=1}^{N-1} a_n \sin n\alpha \qquad (87)$$

where a_n are given explicitly (14) as functions of the values at $\alpha_i = \frac{i\pi}{N}$, $0 \le i \le N$. The meanline offset then becomes

$$\frac{E_c(\alpha_o, x_R)}{D} = \sum_{n=1}^{N-1} a_n \frac{1 - \cos n\alpha_o}{n} \qquad (88)$$

which can be rearranged in the form:

$$\frac{E_c(\alpha_o, x_R)}{D} = \sum_{i=1}^{N-1} \left(\frac{\partial \frac{E_c}{D}}{\partial x_c} \cdot \frac{\sin\alpha}{2} \right)_{\alpha_i} T_i(\alpha_o) \qquad (89)$$

where $T_i(\alpha_o)$ are a set of coefficients dependent on the interval spacing and desired evaluation point α_o. They can be calculated once and for all and stored for repeated use. Similar procedures are followed for all regular integrations.

For the integral with a singular point, the Cauchy Principal Value must be obtained (see Equation 28). First the integration in the radial direction is performed, resulting in an equation

$$\frac{\underline{v}(\alpha_o, x_{R_o})}{V} = \frac{1}{\pi} \int_0^{\pi} \underline{F}(\alpha; \alpha_o, x_{R_o}) \frac{d\alpha}{\cos\alpha - \cos\alpha_o} \qquad (90)$$

The regular part of the integrand, $\underline{F}(\alpha; \alpha_o, x_{R_o})$ can be expanded in a half-range cosine series in α:

$$\underline{F}(\alpha; \alpha_o, x_{R_o}) = \sum_{n=0}^{N} \underline{a}_n(\alpha_o, x_{R_o}) \cos n\alpha \qquad (91)$$

and the integral evaluated analytically (15):

$$\frac{\underline{v}}{V} = \frac{1}{\pi} \int_0^{\pi} \frac{\underline{F}(\alpha; \alpha_o, x_{R_o})\, d\alpha}{\cos\alpha - \cos\alpha_o} \qquad (92)$$

$$= \frac{1}{\pi} \sum_{n=0}^{N} a_n \int_0^{\pi} \frac{\cos n\alpha\, d\alpha}{\cos\alpha - \cos\alpha_o}$$

$$= \sum_{n=1}^{N} a_n \frac{\sin n\alpha_o}{\sin\alpha_o} \qquad (93)$$

The numerical procedure consists of evaluating the coefficients a_n in terms of values of the integrand (Equation 91) at equal angular intervals of α from 0 to π. Finally, Equation (93) is rearranged to be the sum of the product of the integrand values at discrete points and coefficients R_m which can be determined once and for all:

$$\frac{\underline{v}}{V} = \sum_{m=0}^{N} \left[\underline{F}(\alpha; \alpha_o, x_{R_o}) \right]_{\frac{m\pi}{N}} \cdot R_m(\alpha_o) \qquad (94)$$

where $(\underline{F})_{\frac{m\pi}{N}}$ are a table of values of Equation (91) at $\alpha = \frac{m\pi}{N}$, $0 \le m \le N$, and $R_m(\alpha_o)$ are a set of coefficients dependent on the interval spacing as well as the desired evaluation points, α_o. Details of this procedure as well as FORTRAN statements for a computer subroutine are given in Reference 16.

To determine a value of the radial integrand at the singular point $x_c = x_{c_o}$, a linear expansion of the position vector $\underline{s}_o$ about the fixed point $\underline{r}_o$ is derived. This linear expansion results in a form of the integrand which can be integrated analytically in the radial direction by holding the other terms in the integral constant at x_{R_o}. The expansion of $\underline{s}_o$ about $\underline{r}_o$ produces the equation

$$\frac{\underline{s}_o}{D} = \frac{\underline{r}_o}{D} + (x_R - x_{R_o}) \left(\frac{\partial \frac{\underline{s}_o}{D}}{\partial x_R} \right)_{\underline{r}_o} + (x_c - x_{c_o}) \left(\frac{\partial \frac{\underline{s}_o}{D}}{\partial x_c} \right)_{\underline{r}_o} + \cdots \qquad (95)$$

$$= \frac{\underline{r}_o}{D} + (x_R - x_{R_o}) \left(\alpha \underline{e}_1 + \frac{1}{2} \frac{\underline{N}_o^+ \times \underline{e}_1}{\frac{D^2}{2} \frac{c}{D}} \right)_{\underline{r}_o}$$

$$+ (x_c - x_{c_o}) \frac{c}{D} \underline{e}_1 + \cdots \qquad (96)$$

The approximate distance from the reference point is

$$|\underline{r}_o - \underline{s}_o| \approx \rho(x_R - x_{R_o}, x_{c_o} - x_c) \cdot D$$

where

$$\rho(x_R, x_c) = \sqrt{A x_R^2 + B x_R x_c + \left(\frac{c}{D}\right)^2 x_c^2} \qquad (97)$$

and $A(x_{c_o}, x_{R_o})$ and $B(x_{c_o}, x_{R_o})$ are

$$A = \frac{1}{4} + \left(\frac{di_T/D}{dx_R}\right)^2 + 2\left(\frac{di_T/D}{dx_R}\right)(x_c - 0.5)\frac{d}{dx_R}\left(\frac{c}{D}\sin\phi_P\right)$$

$$+ (x_c - 0.5)^2\left\{\left[\frac{d}{dx_R}\left(\frac{c}{D}\sin\phi_P\right)\right]^2 + \left(\frac{x_R}{2}\frac{\partial\theta(x_c, x_R)}{\partial x_R}\right)^2\right\} \quad (98)$$

and

$$B = 2\left\{-\frac{c}{D}\sin\phi_P\left[\frac{d}{dx_R}\left(\frac{c}{D}\sin\phi_P\right)(x_c - 0.5) + \frac{di_T/D}{dx_R}\right]\right.$$

$$\left. - \frac{x_R}{2}\frac{c}{D}\cos\phi_P\frac{\partial\theta(x_c, x_R)}{\partial x_R}\right\} \quad (99)$$

The linearized integrand $\underline{F}$, for integration over the blade reference surface, then becomes, in the general form (where a_i, b_i, and $\hat{e}_i$, depend on the particular case of loading or thickness):

$$\underline{F} = (x_{c_o} - x_c)\sum_{i=1}^{3}\int_{x_h}^{1} dx_R \quad (100)$$

$$\cdot \frac{\left[(x_R - x_{R_o})\,a_i + (x_{c_o} - x_c)\,b_i\right]\hat{e}_i}{\left[A(x_R - x_{R_o})^2 + B(x_R - x_{R_o})(x_{c_o} - x_c) + \left(\frac{c}{D}\right)^2(x_{c_o} - x_c)^2\right]^{3/2}}$$

$$= \sum_{i=1}^{3}(a_i D_1 + b_i D_2)\,\hat{e}_i$$

where

$$D_1 = \int_{x_h}^{1}\frac{(x_{c_o} - x_c)(x_R - x_{R_o})\,dx_R}{\left[\rho(x_R - x_{R_o}, x_{c_o} - x_c)\right]^3}$$

$$= -\frac{2}{\left[4A\left(\frac{c}{D}\right)^2 - B^2\right]} \quad (101)$$

$$\cdot \left[\frac{B(1 - x_{R_o}) + 2\left(\frac{c}{D}\right)^2(x_{c_o} - x_c)}{\sqrt{A(1 - x_{R_o})^2 + B(1 - x_{R_o})(x_{c_o} - x_c) + \left(\frac{c}{D}\right)^2(x_{c_o} - x_c)^2}}\right.$$

$$\left. - \frac{B(x_h - x_{R_o}) + 2\left(\frac{c}{D}\right)^2(x_{c_o} - x_c)}{\sqrt{A(x_h - x_{R_o})^2 + B(x_h - x_{R_o})(x_{c_o} - x_c) + \left(\frac{c}{D}\right)^2(x_{c_o} - x_c)^2}}\right]$$

and

$$D_2 = \int_{x_h}^{1}\frac{(x_{c_o} - x_c)^2\,dx_R}{\left[\rho(x_R - x_{R_o}, x_{c_o} - x_c)\right]^3}$$

$$= \frac{2}{\left[4A\left(\frac{c}{D}\right)^2 - B^2\right]} \quad (102)$$

$$\cdot \left[\frac{2A(1 - x_{R_o}) + B(x_{c_o} - x_c)}{\sqrt{A(1 - x_{R_o})^2 + B(1 - x_{R_o})(x_{c_o} - x_c) + \left(\frac{c}{D}\right)^2(x_{c_o} - x_c)^2}}\right.$$

$$\left. - \frac{2A(x_h - x_{R_o}) + B(x_{c_o} - x_c)}{\sqrt{A(x_h - x_{R_o})^2 + B(x_h - x_{R_o})(x_{c_o} - x_c) + \left(\frac{c}{D}\right)^2(x_{c_o} - x_c)^2}}\right]$$

At the singular point $x_c \to x_{c_o}$,

$$\underline{F}(x_{c_o}; x_{R_o}, x_{c_o}) = 4\frac{\sum_{i=1}^{3}\{-a_i B + 2b_i A\}\,\hat{e}_i}{\sqrt{A}\left[4A\left(\frac{c}{D}\right)^2 - B^2\right]} \quad (103)$$

This known value at the singular point allows a straightforward analysis procedure to be undertaken using the procedures previously described.

Some convergence problems near the leading and trailing edges and over much of the surface for narrow blades (maximum $c/D \approx 0.05$) have been resolved by computing the linearized form of F (Equation 100) over the entire blade and adding a correction term which is the difference between the actual integrand and this linear approximation. This option has been included in the computer program and is defined as "linear approximation-plus-difference." When conventional integration techniques are used everywhere except at the singular point, where Equation (103) is required, the procedure is defined as "direct."

For the trailing-vortex sheet, a regular integration can be performed since no singular points occur on the sheet. The strength of the vorticity is given by Equation (59) and the induced velocity field is given by

$$\frac{\underline{v}}{V} = \frac{1}{4}\int_0^1\left(-\frac{dG}{dx_R}\right)\sum_{b=1}^{Z}\underline{W}(\underline{r}_o, x_R, \theta_b)\,dx_R \quad (104)$$

where

$$\underline{W}(\underline{r}_o, x_R, \theta_b) = \int_0^\infty \underline{e}_1 \times \frac{\frac{\underline{r}_o}{D} - \frac{\underline{s}w_b}{D}}{\left|\frac{\underline{r}_o}{D} - \frac{\underline{s}w_b}{D}\right|^3}\,d\eta \quad (105)$$

For the case when the field point $\underline{r}_o$ is given in cylindrical polar coordinates,

$$\left.\begin{aligned} \frac{\underline{r}_o}{D}\left(\frac{x_o}{D}, x_{R_o}, \phi\right) &= \frac{x_o}{D}\,\underline{i} + \frac{x_{R_o}}{2}\,\underline{e}_r(\phi) \\ \text{and} \\ \frac{\underline{S}_{W_b}}{D}(\eta, x_R) &= \frac{x(\eta, x_R)}{D}\,\underline{i} + \frac{x_R}{2}\,\underline{e}_r\left(\theta(\eta, x_R) + \theta_b\right) \end{aligned}\right\} \quad (106)$$

where

$$\left.\begin{aligned} \frac{x(\eta, x_R)}{D} &= \frac{x_{te}}{D} + \eta \sin\phi_P \\ \theta(\eta, x_R) &= \theta_{te} + 2\eta\cos\phi_P/x_R \end{aligned}\right\} \quad (107)$$

Then

$$\begin{aligned} \underline{e}_1 \times \left(\frac{\underline{r}_o}{D} - \frac{\underline{S}_{W_b}}{D}\right) &= \frac{\cos\phi_P}{2}\left[x_R - x_{R_o}\cos(\theta + \theta_b - \phi)\right]\,\underline{i} \\ &+ \left[\left(\frac{x_o}{D} - \frac{x}{D}\right)\cos\phi_P \sin(\theta + \theta_b - \phi)\right. \\ &\left. + \frac{\sin\phi_P}{2}\left(x_{R_o} - x_R\cos(\theta + \theta_b - \phi)\right)\right]\underline{e}_\phi \\ &+ \left[\left(\frac{x_o}{D} - \frac{x}{D}\right)\cos\phi_P\cos(\theta + \theta_b - \phi)\right. \\ &\left. + \sin\phi_P\frac{x_R}{2}\sin(\theta + \theta_b - \phi)\right]\underline{e}_r(\phi) \\ &= \frac{\cos\phi_P}{2}\left[x_R - x_{R_o}\cos\left(\theta_{te} + \theta_b - \phi\right.\right. \\ &\left.\left. + 2\eta\frac{\cos\phi_P}{x_R}\right)\right]\,\underline{i} + \left[\left(\frac{x_o - x_{te}}{D}\right.\right. \\ &\left.\left. - \eta\sin\phi_P\right)\cos\phi_P\sin\left(\theta_{te} + \theta_b - \phi\right.\right. \\ &\left.\left. + 2\eta\frac{\cos\phi_P}{x_R}\right) + \frac{\sin\phi_P}{2}\left(x_{R_o}\right.\right. \\ &\left.\left. - x_R\cos\left(\theta_{te} + \theta_b - \phi + 2\eta\frac{\cos\phi_P}{x_R}\right)\right)\right]\underline{e}_\phi \\ &+ \left[\left(\frac{x_o - x_{te}}{D} - \eta\sin\phi_P\right)\cos\phi_P\cos\left(\theta_{te}\right.\right. \\ &\left.\left. + \theta_b - \phi + 2\eta\frac{\cos\phi_P}{x_R}\right) + \frac{\sin\phi_P}{2}x_R\sin\left(\theta_{te}\right.\right. \\ &\left.\left. + \theta_b - \phi + 2\eta\frac{\cos\phi_P}{x_R}\right)\right]\underline{e}_r(\phi) \end{aligned} \quad (108)$$

A computer code has been developed for a subroutine to compute the approximate value of $\underline{W}$:

$$\underline{W} = \int_0^{\eta_1} \underline{e}_1 \times \frac{\frac{\underline{r}_o}{D} - \frac{\underline{S}_{W_b}}{D}}{\left|\frac{\underline{r}_o}{D} - \frac{\underline{S}_{W_b}}{D}\right|^3}\,d\eta + \int_{\eta_1}^{\eta_2} \underline{e}_1 \times \frac{\frac{\underline{r}_o}{D} - \frac{\underline{S}_{W_b}}{D}}{\left|\frac{\underline{r}_o}{D} - \frac{\underline{S}_{W_b}}{D}\right|^3}\,d\eta \quad (109)$$

Options are included in the subroutine call statement to permit the first integral to be evaluated either by the trapezoidal rule with equal increments in η or by Simpson's rule with equal increments in $\sqrt{\eta}$. This second integration procedure insures more dense spacing of the integrand near the blade and a more accurate computation. To insure an even number of intervals, the number of points specified in the call statement is doubled when this more accurate procedure is employed. The second integral is evaluated by the trapezoidal rule but is not employed when $\eta_2 \leq \eta_1$.

For a given value of η_1 and specified number of double intervals, N, the constant increment in $\sqrt{\eta}$ is

$$\Delta\sqrt{\eta} = \frac{\sqrt{\eta_1}}{2N}$$

for which the increment in η between successive points is

$$\begin{aligned} \Delta\eta_i &= \eta_i - \eta_{i-1} \\ &= (2i - 1)\frac{\eta_1}{4N^2} \end{aligned} \quad (110)$$

and the increment in angular variable θ between successive points is

$$\begin{aligned} \Delta\theta_i &= 2\Delta\eta_i\cos\phi_P/x_R \\ &= (2i - 1)\,2\cos\phi_P\,\eta_1/(x_R\,4N^2) \end{aligned} \quad (111)$$

from which

$$\Delta\theta_1 = \frac{\eta_1}{4N^2}\,\frac{2\cos\phi_P}{x_R}$$

and

$$\Delta\theta_{2N} = \frac{4N - 1}{4N^2}\,\eta_1\,\frac{2\cos\phi_P}{x_R} = (4N - 1)\,\Delta\theta_1$$

Generally $\eta_1 = \eta_2$ and the equal increments of $\sqrt{\eta}$ are used for integration with $N = 2 \cdot \eta_2$ double intervals. A value of $\eta_2 = 10$ has been satisfactory to date. When the distance between points becomes small, special fine point spacing in η is employed to insure convergence. Accuracy of calculations was determined by comparison with analytical results for the tangential velocity component due to a circular arc vortex filament, the axial velocity component at the origin for a general helical filament, all velocity components for a straight line vortex, and induction factors (17) for general helical filaments. At individual points of this comparison for filaments, accuracy to the third decimal point was found with the selected parameters and an overall accuracy of the non-dimensional induced velocity component of the sheet to one or two units in the fourth decimal point was found.

In order to perform calculations, the form of γ^* and non-dimensional thickness must also be specified. A general family of loading functions has been selected (18) with the property that they have zero values at the leading and trailing edges and resemble conventional NACA loading functions (19). The zero values at the ends are necessary for accurate fit with a sine-series trigonometric interpolation polynomial. For loading distributions which approximate the NACA a series meanlines, the following chordwise form is used

$$\gamma = \begin{cases} (\sin\alpha)^{1/K} & 0 \le x_c \le 0.5 \\ 1.0 & 0.5 \le x_c \le b,\ 0.5 \le b \le 1.0 \\ 1 - \left(\dfrac{x_c - b}{1 - b}\right)^2 & b \le x_c \le 1.0 \end{cases} \tag{112}$$

where

$$x_c = \frac{1}{2}(1 - \cos\alpha)$$

The value of K can be taken sufficiently large to make the load distribution in the leading-edge region nearly rectangular. A previous investigation (18) of this loading function for K = 8 and b = 0.7 demonstrated that it was an acceptable approximation of the NACA a = 0.8 meanline, see Figure 2. Symmetrical chordwise loading functions were selected to be

$$\gamma = (\sin\alpha)^{1/K} \qquad 0 \le x_c \le 1 \tag{113}$$

Each selected load distribution must be integrated across the chord and scaled to produce a unit value for the integral.

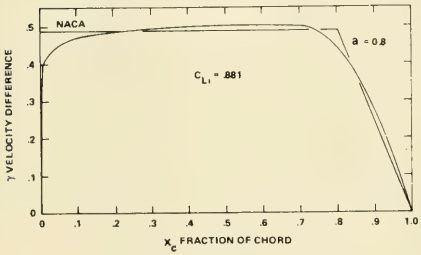

Fig. 2 Load distribution

The thickness offset is assumed in the form

$$\frac{E_T}{D} = \frac{c(x_R)}{D} \cdot \frac{t}{c}(x_R) \cdot Y_T(x_c) \tag{114}$$

where the chordwise distribution, $Y_T(x_c)$, remains the same from root to tip, only the maximum value changes with radius. This is true for current propulsor designs. Specific examples of the thickness function included in the computer code are the NACA 4 and 5 digit sections (19), the NACA 16 section (20), an elliptic nose quartic tail section similar to that described in Reference 21, and an approximate NACA 66 (Mod) (22) section. All have been analytically defined.

Computer Code Convergence and Run Time

The complexity of the numerical analysis is such that error estimates are difficult to establish. A few limiting cases exist for which analytic integrations may be performed but comparisons do not usually evaluate the general case. The procedure selected to evaluate convergence was to vary the number of intervals in the radial direction, NR, and the number of intervals in the chordwise direction, NX. In addition, some radii and chordwise points were eliminated from the calculations. Computed values of the pitch and camber at selected radii are shown in Table I, together with a similar variation of data calculated according to the procedure described in Reference 7 for the same propulsor which is similar to NSRDC Model 4498. Computer central processing time is for computations at 13 radii between the extreme radii listed and is in seconds for the Burroughs 7700 High-Speed Computer. Current charges are 3 cents per CPU second, resulting in a maximum charge of about $40. All procedures presented produce about equally satisfactory results with about only one percent difference in pitch or camber values, about the same as found for Kerwin's numerical analysis. The computed pitch, however, is a few percent less than computed by Kerwin's method. Since unpublished experience at DTNSRDC to date has been that Kerwin's procedure produces designs that are generally slightly overpitched perhaps some improvement in performance may be expected using the present method.

Predictions of the pitch and camber by the two procedures developed for computing the induced velocity field on the blade surface which contains the field point, "direct" and "approximate-plus-difference," are shown in Table I to be nearly the same. However, it has been found that overall, the "approximate-plus-difference" procedure is preferable when dense chordwise spacing is chosen (e.g., NX = 19) or narrow blades (maximum $c/D \approx 0.05$) are involved. In these situations, the "direct" procedure produces locally erratic values of the induced velocity because of the decreased spacing between adjacent lines of integration with a corresponding lack of accuracy in the numerical integrations for the resulting near-singular integrals. This effect is illustrated in Figure 3 which shows values of one of the helical components of the average induced velocity at the 0.946 radius of the reference blade. This velocity component is due to only loading on the blade itself; the effects of thickness, the other blades and the shed vortex sheet are not included. All data shown in subsequent figures have been computed by the "approximate-plus-difference" procedure although only the pressure distribution near the leading edge in the tip region of the blade was significantly different between the two procedures.

Overall run time varies with number of points, number of blades, and blade width. Since computer usage charges are so low, the 181 x 19 array size is recommended. For a narrow blade, the linear "approximation-plus-difference" procedure is recommended, and the run time may increase by a few hundred seconds because of special care taken with the shed vortex sheet calculations. Computer execution time for Kerwin's program is unknown for the Burroughs 7700 high-speed computer but is estimated to be about 150 seconds, for data calculations at 4 chordwise points at 8 radial stations. For the results shown in Table I, data are computed at 13 radial stations with either 8, 11 or 17 chordwise points, depending on input data specification.

Further details of the geometry of this example are given in Table II. Radial variables are titled according to the symbols suggested in Reference 10.

Table I
Effect of Parameters on Pitch, Camber and Computer Run Time

x_R	COMPUTATIONAL PROCEDURE: 91 x 10 Direct	181 x 10 Direct	181 x 13 Direct	91 x 19 Direct	181 x 19 Direct	91 x 19 Approx + Diff	181 x 19 Approx + Diff	Kerwin Computation (7) $\Delta\theta = 2°, M = 52$	Kerwin Computation (7) $\Delta\theta = 2°, M = 70$
					PITCH/DIAMETER				
0.25	–	–	–	–	–	–	–	1.580	1.603
0.254	1.495	1.495	1.517	1.537	1.538	1.539	1.540	1.576	
0.4	1.466	1.466	1.477	1.487	1.487	1.487	1.488	1.511	1.523
0.6	1.264	1.264	1.271	1.277	1.277	1.277	1.277	1.292	1.296
0.669	1.184	1.184	1.189	1.194	1.193	1.193	1.193	1.213	
0.8	1.038	1.038	1.040	1.043	1.042	1.042	1.042	1.065	1.070
0.946	0.883	0.882	0.882	0.884	0.883	0.883	0.883	0.894	
0.95	–	–	–	–	–	–	–	0.890	0.885
					CAMBER/CHORD				
0.25	–	–	–	–	–	–	–	0.0266	0.0259
0.254	0.0305	0.0305	0.0315	0.0320	0.0322	0.0323	0.0324	0.0268	–
0.4	0.0365	0.0365	0.0367	0.0368	0.0368	0.0369	0.0369	0.0350	0.0351
0.6	0.0291	0.0291	0.0293	0.0295	0.0295	0.0295	0.0295	0.0301	0.0294
0.669	0.0255	0.0255	0.0257	0.0257	0.0258	0.0254	0.0257	0.0257	–
0.8	0.0189	0.0189	0.0189	0.0188	0.0189	0.0188	0.0188	0.0181	0.0180
0.946	0.0124	0.0124	0.0122	0.0122	0.0123	0.0123	0.0122	0.0122	–
0.95	–	–	–	–	–	–	–	0.0120	0.0113
CPU Time, Seconds	310	420	600	735	1085	785	1135	N/A	N/A

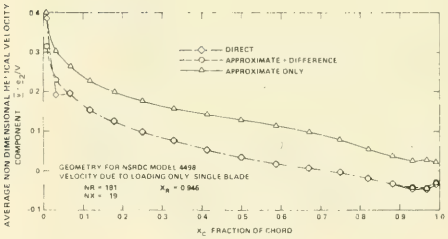

Fig. 3 Helical velocity component, $\underline{v} \cdot \underline{e}_2 / V$

DISCUSSION OF EXAMPLE COMPUTATIONS

In this section, the consequences of choices the designer might make both for overall geometry and for the chordwise variation of the thickness distribution and loading distribution are examined. Some common variations in the location of the blade mid-chord line are investigated to determine the effects of overall geometry on pitch, camber, pressure distribution, and second-order performance coefficients. The variations are unskewed, skewed and warped (23) blades with other input specifications the same. Skewed blades have blade-sections displaced along the pitch helix and warped blades have blade sections displaced circumferentially in the plane at $x = 0$.

Input quantities and selected output are shown in Table II for a warped blade similar to NSRDC Model 4498 (and one similar to the example of Reference 7). For an unskewed blade, the column labeled TETS, the skew angle θ_s, would be zero, and for a skewed blade the column labeled RAKT/D, the total rake i_T/D, would be equal to $P \cdot \theta_s/(2\pi D)$. In Figure 4, the computed pitch and camber ratios are shown for these various overall geometries with all other input the same as in Table II. In Figure 5, the effects of the chordwise load distribution and chordwise thickness function on pitch and camber are shown. The effect of rake and skew on pitch and camber follows known trends (7, 24). The effect of thickness distribution on pitch and camber is negligible and the effect of elliptic loading is to reduce the pitch and increase the camber, as would be the case in two dimensional flow at the ideal angle for a given lift coefficient. In Figure 6, the pitch and camber change is shown for another modification of the warped blade. Since a large change occurs in the pitch from the input specification (Table II) to the computed values (Figure 4), computations were performed with the singularities distributed on the blade reference surface at a pitch taken from Figure 4. This change in pitch places the singularities nearer the final blade surface. To have uniformity in the calculations, the pitch angle of the shed vortex sheet was taken as β, the advance angle of the shed vortex sheet. (In Figure 4, the shed vortex sheet was taken to be at the input pitch, which is β_i, the pitch angle derived from the solution of a straight radial lifting-line representing each blade.) The change in pitch angle of the shed vortex wake from β_i to β produces a slight increase of pitch near the hub (compare data in Figures 4 and 6). A change in the pitch of the blade reference surface to the values shown by the dashed curve in Figure 4 produces a significant reduction in computed pitch and a compensating increase in camber near the root, with negligible change in either pitch or camber from about $x_R = 0.5$ to the tip. Hence the orientation of the free vortex sheet and blade reference surface have significant effects on the pitch and camber values only near the hub.

Table II
DEFINITION OF DESIGN EXAMPLE
Sample Data from Computer Code

4498 EXAMPLE LOADING AND THICKNESS, 5 BLADES - SEPT 80

CIRCULATION COEFFICIENTS

N	G(N)
1	0.029028
2	0.002010
3	-0.002830
4	-0.000540
5	0.000081
6	0.000081

DIAMETER = DP = 0.3048 M ADVCV = V/(ND) = 0.8880 NPB = Z = 5

INPUT DATA

XR	CH/DP	PP/DP	RAKT/DP	TETS	TMAX/CH
0.20000	0.16500	1.16270	0.00000	0.00000	0.24000
0.25000	0.19700	1.19530	0.00000	0.07854	0.19800
0.30000	0.22900	1.22790	0.00000	0.15708	0.15610
0.40000	0.27500	1.25980	0.00000	0.31416	0.18680
0.50000	0.31200	1.25570	0.00000	0.47124	0.07680
0.60000	0.33700	1.21600	0.00000	0.62832	0.05650
0.70000	0.34700	1.15960	0.00000	0.78540	0.04210
0.80000	0.33400	1.09870	0.00000	0.94248	0.03140
0.90000	0.28000	1.03570	0.00000	1.09956	0.02460
0.95000	0.24000	1.00460	0.00000	1.17810	0.02330
1.00000	0.00000	0.97350	0.00000	1.25664	0.02460

4498 EXAMPLE LOADING AND THICKNESS, 5 BLADES - SEPT 80

XR	CH/DP	(CH/DP)'	PP/DP	(PP/DP)'	RAKT/DP	TETS	(TETS)'	TMAX/CH	(TMAX/DP)'	VX/V
0.20000	0.16500	0.62731	1.16270	0.63958	0.00000	0.00000	1.57080	0.24000	-0.82618	1.00000
0.20608	0.16882	0.62982	1.16659	0.64013	0.00000	0.00955	1.57080	0.23498	-0.82679	1.00000
0.22412	0.18020	0.63875	1.17820	0.64825	0.00000	0.03789	1.57080	0.21999	-0.83583	1.00000
0.25359	0.19936	0.65792	1.19774	0.66124	0.00000	0.08418	1.57080	0.19488	-0.87251	1.00000
0.29358	0.22516	0.68910	1.22416	0.68024	0.00000	0.14700	1.57080	0.16097	-0.77784	1.00000
0.34288	0.25127	0.76041	1.24706	0.73807	0.00000	0.22444	1.57080	0.13002	-0.49729	1.00000
0.40000	0.27500	0.39203	1.25980	0.12505	0.00000	0.31416	1.57080	0.10680	-0.34834	1.00000
0.46319	0.29924	0.36619	1.26143	-0.08322	0.00000	0.41342	1.57080	0.08667	-0.28746	1.00000
0.53054	0.32119	0.27819	1.24678	-0.34858	0.00000	0.51921	1.57080	0.06970	-0.21753	1.00000
0.60000	0.33700	0.17799	1.21600	-0.51413	0.00000	0.62832	1.57080	0.05650	-0.16708	1.00000
0.66946	0.34573	0.06936	1.17761	-0.58232	0.00000	0.73743	1.57080	0.04606	-0.13522	1.00000
0.73681	0.34594	-0.07546	1.13751	-0.60499	0.00000	0.84322	1.57080	0.03775	-0.11189	1.00000
0.80000	0.33400	-0.23023	1.09870	-0.62392	0.00000	0.94248	1.57080	0.03140	-0.08871	1.00000
0.85712	0.30705	-0.59158	1.06273	-0.63250	0.00000	1.03220	1.57080	0.02699	-0.06529	1.00000
0.90642	0.27597	-0.62509	1.03169	-0.62442	0.00000	1.10964	1.57080	0.02432	-0.04245	1.00000
0.94641	0.24451	-1.18469	1.00683	-0.62063	0.00000	1.17246	1.57080	0.02330	-0.00309	1.00000
0.97588	0.18588	-3.11163	0.98852	-0.62218	0.00000	1.21875	1.57080	0.02375	0.02963	1.00000
0.99392	0.10001	-7.85659	0.97728	-0.62256	0.00000	1.24709	1.57080	0.02437	0.03749	1.00000
1.00000	0.00000	-99.59900	0.97350	-0.62258	0.00000	1.25664	1.57080	0.02460	0.03802	1.00000

4498 EXAMPLE LOADING AND THICKNESS, 5 BLADES - SEPT 80

ELLIPSE WITH AIRFOIL TAIL AND CHORDWISE LOAD

XC	YT	DY/DANG	SINANG	COSANG	2D U/V	GAM *	GAMINT	2D YC
0.000000	0.000000	0.500000	0.000000	1.000000	1.004224	0.000000	0.000000	0.000000
0.007596	0.086824	0.492404	0.173648	0.984808	1.005031	0.912003	0.005193	0.007943
0.030154	0.171010	0.469846	0.342020	0.939693	1.004562	0.992645	0.027568	0.024846
0.066987	0.250000	0.433013	0.500000	0.866025	1.005799	1.040899	0.064678	0.046076
0.116978	0.321394	0.383022	0.642788	0.766044	1.005783	1.074103	0.117962	0.069016
0.178606	0.383022	0.321394	0.766044	0.642788	1.007820	1.097916	0.184685	0.091134
0.250000	0.433013	0.250000	0.866025	0.500000	1.008799	1.114882	0.263946	0.110726
0.328990	0.469846	0.171010	0.939693	0.342020	1.012858	1.126317	0.352310	0.126081
0.413176	0.492404	0.086824	0.984808	0.173648	1.017103	1.132938	0.447614	0.136207
0.500000	0.500000	-0.000000	1.000000	-0.000000	1.029601	1.135109	0.545946	0.140136
0.586824	0.492202	-0.091113	0.984808	-0.173648	1.055582	1.135109	0.644652	0.137606
0.671010	0.467219	-0.178511	0.939693	-0.342020	1.095197	1.135109	0.740083	0.128200
0.750000	0.421900	-0.322508	0.866025	-0.500000	1.092884	1.103578	0.829166	0.111395
0.821394	0.354824	-0.442816	0.766044	-0.642788	0.998106	0.949248	0.903254	0.086967
0.883022	0.269637	-0.523366	0.642788	-0.766044	0.721556	0.712632	0.954948	0.059375
0.933013	0.176665	-0.526605	0.500000	-0.866025	0.229548	0.453324	0.984272	0.033869
0.969846	0.091629	-0.430943	0.342020	-0.939693	-0.610899	0.216717	0.996676	0.014687
0.992404	0.031655	-0.243206	0.173648	-0.984808	-1.593591	0.056755	0.999765	0.003451
1.000000	0.010000	-0.143374	0.000000	-1.000000	-2.014223	0.000000	1.000000	0.000000

IDEAL ANGLE * 2.454 DEG

Table II. (Cont.)
SOME COMPUTED VARIABLES

XR = 0.254

XC	CP UP	CP LO	DEC/DX	UHELI	VHELI	UR
0.0076	0.2804	0.3421	0.0201	0.4200	-0.0755	-0.0423
0.0302	0.9931	-0.3451	0.0096	0.4172	-0.1401	-0.0290
0.0670	1.3001	-0.3442	0.0045	0.4089	-0.1755	-0.0328
0.1170	1.4419	-0.7406	0.0018	0.3957	-0.2140	-0.0348
0.1786	1.4759	-0.7383	0.0059	0.3791	-0.2452	-0.0341
0.2500	1.4674	-0.7492	0.0111	0.3627	-0.2769	-0.0272
0.3290	1.4413	-0.7289	0.0158	0.3475	-0.3048	-0.0181
0.4132	1.4125	-0.7107	0.0205	0.3345	-0.3325	-0.0076
0.5000	1.3866	-0.7006	0.0244	0.3252	-0.3557	0.0014
0.5868	1.3648	-0.7111	0.0283	0.3232	-0.3791	0.0086
0.6710	1.3563	-0.7396	0.0316	0.3298	-0.4005	0.0111
0.7500	1.3560	-0.7487	0.0358	0.3307	-0.4282	0.0120
0.8214	1.1693	-0.7091	0.0391	0.3141	-0.4503	0.0124
0.8830	0.7951	-0.5231	0.0414	0.2548	-0.4620	0.0238
0.9330	0.3109	-0.1764	0.0409	0.1453	-0.4486	0.0599
0.9698	0.2099	0.3464	0.0404	-0.0414	-0.4212	0.1472
0.9924	0.5644	0.6314	0.0374	-0.2533	-0.3694	0.2601

XR = 0.669

CP UP	CP LO	DEC/DX	UHELI	VHELI	UR
0.9311	0.4398	0.0578	0.1195	0.0339	-0.2460
1.3778	0.1862	0.0399	0.1182	-0.0789	-0.1999
1.4865	0.1697	0.0322	0.1160	-0.1286	-0.1819
1.5749	0.1827	0.0243	0.1137	-0.1804	-0.1643
1.5588	0.2032	0.0186	0.1110	-0.2185	-0.1529
1.5716	0.2236	0.0127	0.1082	-0.2581	-0.1409
1.5792	0.2407	0.0078	0.1057	-0.2914	-0.1315
1.5835	0.2538	0.0025	0.1036	-0.3265	-0.1209
1.5890	0.2595	0.0021	0.1025	-0.3578	-0.1116
1.6000	0.2577	0.0074	0.1027	-0.3923	-0.1012
1.6177	0.2498	0.0125	0.1044	-0.4260	-0.0907
1.5907	0.2419	0.0196	0.1023	-0.4689	-0.0711
1.3833	0.1936	0.0265	0.0925	-0.5064	-0.0469
1.0160	0.1780	0.0316	0.0665	-0.5293	-0.0190
0.5222	0.2496	0.0338	0.0213	-0.5293	0.0085
0.1002	0.4789	0.0344	-0.0548	-0.5124	0.0451
0.6994	0.8492	0.0327	-0.1441	-0.4801	0.0793

XR = 0.946

CP UP	CP LO	DEC/DX	UHELI	VHELI	UR
0.6729	0.3509	0.0314	0.0404	0.1952	-0.2943
0.8110	0.2604	0.0245	0.0362	0.1126	-0.2559
0.9310	0.1866	0.0216	0.0459	0.0841	-0.2234
0.9919	0.1721	0.0181	0.0486	0.0390	-0.2102
1.0105	0.1866	0.0160	0.0474	0.0123	-0.2008
1.0101	0.1936	0.0138	0.0470	-0.0158	-0.1898
1.0081	0.1975	0.0121	0.0468	-0.0379	-0.1814
1.0617	0.2013	0.0102	0.0464	-0.0619	-0.1719
1.0751	0.2016	0.0087	0.0462	-0.0808	-0.1649
1.0906	0.1989	0.0072	0.0464	-0.1008	-0.1582
1.1132	0.1902	0.0061	0.0475	-0.1164	-0.1544
1.1054	0.1781	0.0042	0.0472	-0.1393	-0.1450
0.9944	0.1430	0.0020	0.0425	-0.1650	-0.1308
0.7580	0.1466	0.0007	0.0271	-0.1938	-0.1106
0.4043	0.2413	0.0024	-0.0027	-0.2103	-0.0952
0.0930	0.5098	0.0035	-0.0559	-0.2200	-0.0837
0.6316	0.8991	0.0033	-0.1228	-0.2175	-0.0840

MEANLINE SHAPE, FRACTION OF CHORD, EC/CH

EFFECT OF RADIAL INFLOW INCLUDED

XR =	0.25359	0.29358	0.34288	0.40000	0.46315	0.53054	0.60000	0.66946	0.73681	0.80000	0.85712	0.90642	0.94641
XC													
0.0000	0.00000	0.00000	0.00000	0.00000	0.00000	0.00000	0.00000	0.00000	0.00000	0.00000	0.00000	0.00000	0.00000
0.0075	0.00174	0.00197	0.00208	0.00211	0.00207	0.00186	0.00166	0.00146	0.00128	0.00115	0.00106	0.00091	0.00078
0.0100	0.00226	0.00255	0.00268	0.00273	0.00261	0.00240	0.00214	0.00188	0.00164	0.00147	0.00136	0.00116	0.00100
0.0250	0.00494	0.00555	0.00584	0.00593	0.00567	0.00518	0.00459	0.00400	0.00348	0.00309	0.00285	0.00245	0.00210
0.0500	0.00876	0.00977	0.01025	0.01039	0.00993	0.00902	0.00795	0.00689	0.00596	0.00527	0.00484	0.00419	0.00360
0.1000	0.01514	0.01672	0.01746	0.01771	0.01688	0.01529	0.01345	0.01162	0.01001	0.00879	0.00806	0.00704	0.00606
0.1500	0.02018	0.02210	0.02301	0.02336	0.02227	0.02015	0.01771	0.01530	0.01314	0.01147	0.01052	0.00926	0.00797
0.2000	0.02426	0.02637	0.02743	0.02785	0.02655	0.02406	0.02118	0.01831	0.01571	0.01365	0.01252	0.01110	0.00917
0.2500	0.02741	0.02959	0.03070	0.03128	0.02991	0.02711	0.02391	0.02071	0.01774	0.01536	0.01410	0.01257	0.01026
0.3000	0.02974	0.03193	0.03309	0.03375	0.03241	0.02944	0.02604	0.02258	0.01933	0.01669	0.01534	0.01372	0.01108
0.3500	0.03134	0.03350	0.03470	0.03555	0.03421	0.03116	0.02765	0.02402	0.02055	0.01769	0.01627	0.01462	0.01168
0.4000	0.03221	0.03431	0.03556	0.03656	0.03538	0.03229	0.02873	0.02500	0.02138	0.01837	0.01690	0.01523	0.01205
0.4500	0.03242	0.03445	0.03575	0.03690	0.03580	0.03285	0.02932	0.02555	0.02183	0.01872	0.01723	0.01556	0.01220
0.5000	0.03207	0.03400	0.03535	0.03666	0.03574	0.03292	0.02947	0.02571	0.02196	0.01880	0.01730	0.01566	0.01218
0.5500	0.03116	0.03299	0.03440	0.03584	0.03512	0.03247	0.02915	0.02547	0.02175	0.01859	0.01709	0.01549	0.01199
0.6000	0.02968	0.03142	0.03289	0.03445	0.03392	0.03149	0.02834	0.02479	0.02117	0.01806	0.01657	0.01505	0.01162
0.6500	0.02772	0.02936	0.03089	0.03251	0.03217	0.02998	0.02705	0.02367	0.02021	0.01722	0.01577	0.01433	0.01109
0.7000	0.02523	0.02679	0.02835	0.02999	0.02991	0.02788	0.02521	0.02209	0.01886	0.01604	0.01465	0.01333	0.01043
0.7500	0.02211	0.02356	0.02511	0.02669	0.02666	0.02503	0.02268	0.01989	0.01699	0.01443	0.01313	0.01196	0.00954
0.8000	0.01831	0.01959	0.02106	0.02251	0.02259	0.02129	0.01932	0.01696	0.01449	0.01230	0.01116	0.01018	0.00836
0.8500	0.01396	0.01500	0.01629	0.01751	0.01766	0.01672	0.01521	0.01337	0.01143	0.00970	0.00878	0.00803	0.00685
0.9000	0.00916	0.00990	0.01092	0.01183	0.01200	0.01142	0.01041	0.00917	0.00785	0.00667	0.00602	0.00553	0.00489
0.9500	0.00436	0.00471	0.00550	0.00580	0.00593	0.00569	0.00520	0.00459	0.00395	0.00336	0.00303	0.00280	0.00256
0.9750	0.00204	0.00222	0.00253	0.00279	0.00287	0.00277	0.00255	0.00226	0.00195	0.00166	0.00150	0.00139	0.00129
1.0000	0.00000	0.00000	0.00000	0.00000	0.00000	0.00000	0.00000	0.00000	0.00000	0.00000	0.00000	0.00000	0.00000
PP/CP=	1.54000	1.55070	1.52829	1.48767	1.42952	1.35764	1.27700	1.19301	1.11270	1.04177	0.98173	0.92987	0.88345

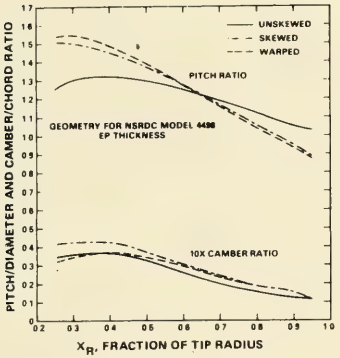

Fig. 4 Effect of skew and rake on pitch and camber values

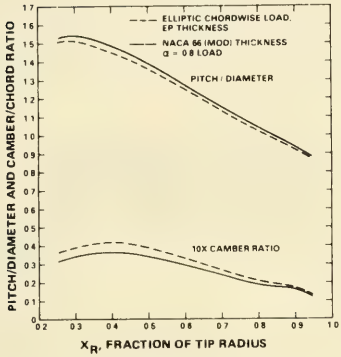

Fig. 5 Effect of chordwise load and thickness on pitch and camber values

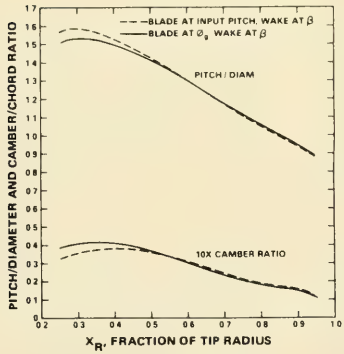

Fig. 6 Effect of orientation of shed vortex sheet and blade reference surface on pitch and camber values

In Figure 7, blade pressure-coefficient distributions on the warped, skewed and unskewed blades are shown for three radii: one near the hub, one near mid-span and one near the tip. The major difference in pressure distributions occurs near the hub, where the warped blades have greater suction on both sides of the blade, and hence a greater tendency to cavitate when the local pressure reaches the vapor pressure.

In Figure 8, the meanline shapes for these blades at the same three radii are shown. The greatest changes in meanline shape occur at the root but are significant all along the radius.

In Figure 9, the non-linear pressure distribution (from Equations (66) and (68)) and meanline shape are shown at x_R = 0.669 for the same variations of chordwise load and thickness distributions shown in Figure 5 for a warped

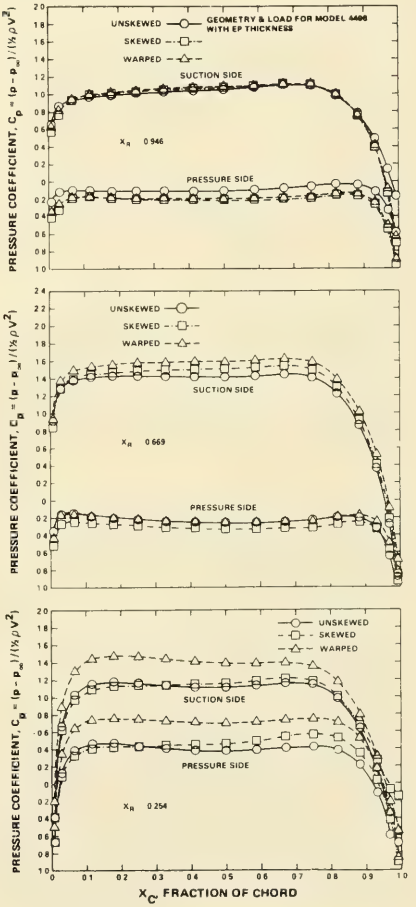

Fig. 7 Pressure distribution at design for three blades

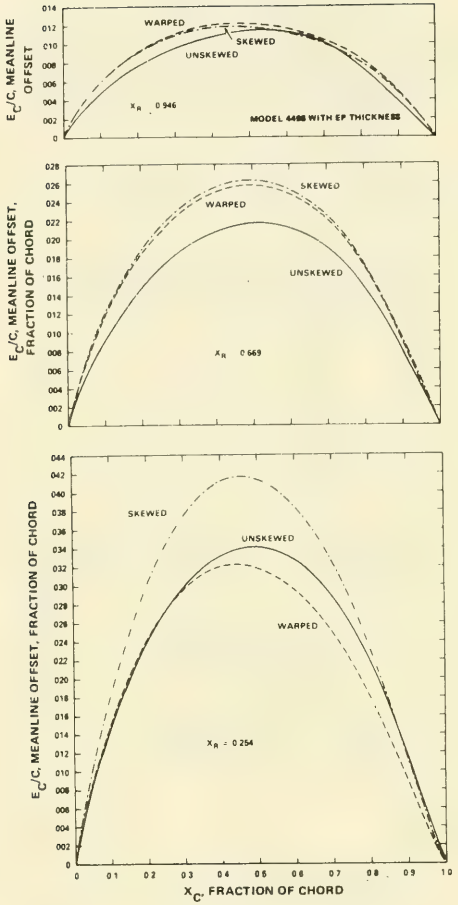

Fig. 8 Meanline shape for three blades

blade similar to NSRDC Model 4498. Both changes in chordwise variables lead to increased suction near mid-chord and reduced suction near the leading edge on the suction side of the blade. An engineering approximation is that cavitation will occur when the minimum pressure on a body equals the vapor pressure of the liquid. Hence at the design point, back bubble cavitation may be degraded by these chordwise variations relative to the conditions of Figure 7 but off-design leading-edge sheet cavitation on the suction side may be improved by these changes in chordwise variables. This conjecture is based on assumed equal incremental changes to the pressure due to off-design operation. Leading edge pressure-side cavitation may be degraded at off-design operation with the elliptic load distribution because of the peak near the leading edge in Figure 9. Meanline shapes are different for these chordwise variations as shown in Figure 9.

Thrust loading and power coefficients (computed from Equations 80 and 81 with $C_D = 0.0085$) are shown in Table III for the various overall geometries and chordwise modifications. The performance coefficients computed according to the lifting-line model and first-order linear lifting-surface model ($E = 0$ in Equations (76) and (78) and ΔC_P from Equation (74)) are nearly identical. The non-linear performance coefficients ($E \neq 0$ in Equations (76) and (80) and C_P from Equation (66)) for a blade with only loading ($E_T = 0$) are increased a few percent relative to the lifting-line values. The addition of thickness and skew or warp changes the pressure distribution and meanline slope, and increases the values by another few percent each, eventually producing values of C_{Th} and C_P which are more than ten percent greater than predicted by the lifting-line model. In both the pressure distribution and force calculations, non-linear, second-order effects have been included in an intrinsically first-order theory. It is not known if the calculated trends with these second-order effects included are valid or not. Experimental evaluation is required to confirm the predictions. Predictions given in Table III should be interpreted as possible trends in the actual performance. The present lifting-line model employed in propeller design (3, 4) assumes a straight radial line with vanishing chordlength to represent the blade and can hardly be expected to be an acceptable model of wide-bladed lifting surfaces, especially ones with skewed or warped blades. Fortunately, the majority of applications to date have generally performed within a few percent of predictions with this simple model but some significant differences have also occurred. Hence both a curved lifting-line and increased-accuracy lifting-surface performance predictions should be developed and evaluated.

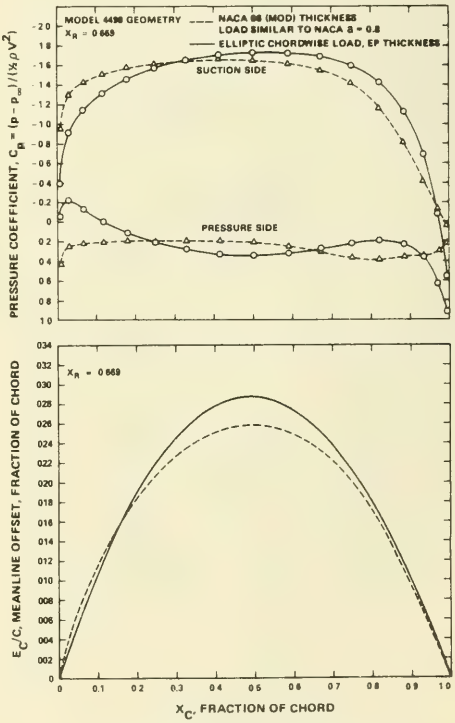

Fig. 9 Pressure distribution and meanline shape for variation of chordwise load and thickness

Table III
Thrust Loading and Power Coefficient

	C_{Th}	C_P	$\eta_o = C_{Th}/C_P$
Lifting Line	0.690	1.016	0.679
1st Order Lifting Surface	0.688	1.013	0.679
Second Order:			
Unskewed,			
Loading Only	0.709	1.030	0.688
Unskewed			
Load & EP thickness	0.736	1.089	0.675
Skewed			
Load & EP thickness	0.783	1.152	0.680
Warped			
Load & EP thickness	0.784	1.148	0.683
Second Order (warped, load and thickness):			
66 thickness	0.782	1.141	0.685
Elliptic load,			
EP thickness	0.782	1.147	0.682
Wake at β	0.790	1.175	0.672
1st Order, Blade at ϕ_g	0.673	1.018	0.661
Second Order, Blade at ϕ_g			
Wake at β	0.794	1.182	0.672

As shown by Huang, et al (25), some wake fields have mean axisymmetric flow velocities with non-zero radial components. In the example body investigated by Huang, a nearly constant value of $w_R = -0.05$ was found. In Table IV, the additive effects of this velocity component are shown. When this w_R component is isolated from Equation (22) and the incremental addition to the meanline denoted by ΔE_c, one finds

$$\frac{\partial \frac{\Delta E_c}{c}}{\partial x_c} = w_R \frac{N_{R_o}}{\sqrt{(1-w_x)^2 + \left(\frac{\pi x_R}{J_v}\right)^2}} \cos(\varphi_P - \beta)$$

$$= \epsilon(x_R) + \delta(x_R) \cdot (x_c - 0.5) \qquad (115)$$

where

$$\epsilon = \frac{w_R}{\sqrt{(1-w_x)^2 + \left(\frac{\pi x_R}{J_v}\right)^2}} \cos(\varphi_P - \beta) \cdot \left\{ 2 \frac{di_T/D}{dx_R} \cos\varphi_P - x_R \frac{d\theta_s}{dx_R} \sin\varphi_P \right\} \qquad (116)$$

$$\delta = \frac{2\, w_R\, c/D}{\sqrt{(1-w_x)^2 + \left(\frac{\pi x_R}{J_v}\right)^2}} \cos(\varphi_P - \beta) \cdot \frac{d\,P/D}{dx_R} \frac{\cos^2\varphi_P}{\pi x_R} \qquad (117)$$

Then

$$\frac{\Delta E_c}{c} = \int_0^{x_c} \frac{\partial \frac{\Delta E_c}{c}}{\partial x_c} dx_c$$

$$= \epsilon x_c - \delta \frac{x_c(1-x_c)}{2} \qquad (118)$$

Thus the ϵ term, due to gradients of the rake and skew of the blade, results in an angle-of-attack change, and the δ term, due to radially variable pitch, results in a parabolic-arc meanline, with a maximum offset at mid chord of

$$\frac{\Delta f}{c} = -\delta/8 \qquad (119)$$

Table IV
EFFECT OF RADIAL VELOCITY COMPONENT
ON PITCH AND CAMBER
(Geometry Similar to NSRDC Model 4498;
$w_R = -0.05$)

x_R	$\left(\frac{f}{c}\right)^*_{Initial}$	$\left(\frac{P}{D}\right)^*_{Initial}$	ϵ	δ	$\frac{\Delta f}{c}$	$\Delta\phi_P$	$\left(\frac{P}{D}\right)_{Final}$
0.4	0.0369	1.488	0.0130	-0.0008	+0.0001	-0.746°	1.449
0.6	0.0295	1.277	0.0110	+0.0026	-0.0003	-0.630°	1.247
0.8	0.0188	1.042	0.0084	+0.0023	-0.0003	-0.481°	1.017

*From Table I, lifting-surface design without effect of w_R.

Table IV shows the effect of $w_R = -0.05$ on the pitch and camber ratio for a warped blade similar to NSRDC Model 4498. The change in camber ratio is probably not significant for this case but the change in pitch angle is important, resulting in a few percent change in the final pitch values. Hence this effect should be included in designs operating in a wake having a significant average radial inflow component.

The present procedure can be improved in several respects: the presence of the hub should be included in the mathematical model, generalized load variations and thickness variations should be included, some physically observed phenomena of the shed vortex sheet should be included, consideration of the radially variable inflow (i.e., free-stream vorticity) should be included, steps to improve the accuracy of computations in the tip region should be undertaken, and program execution time should be shortened. Additionally, similar numerical analysis techniques should be applied to both the performance problem and the determination of unsteady blade response in a non-uniform wake.

Of particular interest is the physically-observed configuration of the free-vortex sheet. As observed by Nelka (23) and modeled by Cummings (26), for highly-skewed blades, an isolated vortex forms along the leading edge of the blade in the tip region. This vortex will influence the induced velocity field and hence produce changes in the pitch, meanline, pressure distribution and force/moment coefficients relative to the model employed herein. In addition, the trailing vortex will contract and roll up. Present models have a vortex sheet starting at the tip rather than somewhere along the leading edge.

Boundary-layer computations on rotating blades performed by Groves (27) utilize output from the computer code described herein. In particular, the pressure distribution, streamline locations, and surface metrics (see Appendix) are input data for the boundary-layer computations.

CONCLUDING REMARKS

Procedures have been described for determining meanline and pitch distributions corresponding to a prescribed load distribution. Computer run times are as great as 20 minutes on the DTNSRDC Burroughs 7700 high-speed computer. Computed meanline and pitch distributions are dependent upon blade mid-chord location and chordwise variation of load distribution, with negligible effect due to chordwise variation of thickness distribution. A radial inflow component was found to have a significant effect on the design pitch of the blades.

Calculated pressure distributions are dependent upon blade rake and skew and both chordwise load distribution and chordwise thickness distribution. Overall performance coefficients calculated from second-order effects show significant differences compared to lifting-line predictions for highly-skewed and warped blades. Experimental confirmation of the predictions is required to evaluate these second-order modifications of a first-order theory.

Suggestions have been given for improving the procedures for calculating design geometry. Some of these suggestions involve an improved mathematical model of the flow field and some are improvements to the numerical analysis techniques.

ACKNOWLEDGEMENTS

The development of the numerical analysis procedures for lifting-surface design was initiated while the author was an Exchange Scientist at the Defence Research Establishment Atlantic, Dartmouth, Nova Scotia and completed at DTNSRDC under work unit 1500-104, Task Area SF43421001, Program element 62543N. The help of Ms. K. Tymchuk and Mr. R. Brian of the DREA staff and Ms. J. Libby of the DTNSRDC staff has been essential to completion of this task.

REFERENCES

1. R. A. Cumming and Wm. B. Morgan, "Propeller Design Aspects of Large High-Speed Ships," Symposium on High Powered Propulsion of Large Ships, Netherlands Ship Model Basin Publication 490, December, 1974.

2. G. G. Cox and Wm. B. Morgan, "The Use of Theory in Propeller Design," Marine Technology, Vol 9, No. 4, October, 1972.

3 E. B. Caster, et al, "A Lifting-Line Computer Program for Preliminary Design of Propellers," DTNSRDC Report SPD-591-01, November, 1975.

4. T. E. Brockett, "A Lifting-Line Computer Program Based on Circulation for Preliminary Hydrodynamic Design of Propellers," Defence Research Establishment Atlantic, Technical Memorandum 79/E, December, 1979.

5. Tsakonas, S., et al, "An 'Exact' Linear Lifting-Surface Theory for a Marine Propeller in a Non-uniform Flow Field," Journal of Ship Research, Vol 17, No. 4, December, 1973.

6. P. van Oossanen, "Calculation of Performance and Cavitation Characteristics of Propellers Including Effects of Non-uniform Flow and Viscosity," Netherlands Ship Model Basin Publication No. 457, 1974.

7. J. E. Kerwin, "Computer Techniques for Propeller Blade Section Design," International Shipbuilding Progress, Vol 20, No. 227, July 1973; also MIT, Dept. of Ocean Engineering, October, 1975.

8. J. F. McMahon, "LFTSUR – A Computer Program for Determining Hydrodynamic Pitch, Meanline Shape, and Pressure Distribution for Marine Propellers," DTNSRDC/SPD-731-01, 1976 (unpublished).

9. Terry Brockett, "Propeller Perturbation Problems," NSRDC Report 3880, October, 1972.

10. H. Lackenby, editor, "International Towing Tank Conference Standard Symbols 1976," British Ship Research Association Technical Memorandum No. 500, May, 1976.

11. A. P. Wills, Vector Analysis with an Introduction to Tensor Analysis, Dover Publications, Inc., 1931.

12. H. B. Phillips, Vector Analysis, Wiley, 1933.

13. J. Weber, "The Calculation of the Pressure Distribution on the Surface of Cambered Wings and the Design of Wings with Given Pressure Distribution," Aeronautical Research Council R&M 3026, 1955.

14. I. S. Sokolnikoff and R. M. Redheffer, Mathematics of Physics and Modern Engineering, McGraw-Hill, 1958.

15. H. Glauert, The Elements of Aerofoil and Airscrew Theory, Cambridge, 1926.

16. Terry Brockett, "A Subroutine for Evaluation of One-Dimensional Singular Integrals (SINGINT)," Defence Research Establishment Atlantic, Technical Memorandum 79/F, December, 1979.

17. W. B. Morgan, "Propeller Induction Factors," DTMB Report 1183, November, 1957.

18. Terry Brockett, "The Design of Two-Dimensional Profiles from a Specified Surface Speed Distribution, Part 1 – Meanline at Ideal Angle of Attack," Defence Research Establishment Atlantic, Technical Memorandum 79/G, December, 1979.

19. I. H. Abbott, and A. E. von Doenhoff, Theory of Wing Sections, Dover, 1959.

20. W. F. Lindsey, et al, "Aerodynamic Characteristics of 24 NACA-16 Series Airfoils at Mach Numbers between 0.3 and 0.8," NACA TN 1546, September, 1948.

21. H. P. Rader, "Cavitation of Propeller Blade Sections," Admiralty Experimental Works, Hasler, Report 22/54, March, 1954.

22. Terry Brockett, "Minimum Pressure Envelopes for Modified NACA-66 Sections with NACA a = 0.8 Camber and BuShips Type I and Type II Sections," DTMB Report 1780, February, 1966.

23. J. J. Nelka, "Experimental Evaluations of a Series of Skewed Propellers with Forward Rake," NSRDC Report 4113, July, 1974.

24. R. A. Cumming, et al, "Highly Skewed Propellers," Trans. SNAME, Vol 80, 1972.

25. T. T. Huang, et al, "Stern Boundary-Layer Flow on Axisymmetric Bodies," Twelfth Symposium on Naval Hydrodynamics, National Academy of Sciences, Wash. D.C., 1978.

26. Damon E. Cummings, "Numerical Prediction of Propeller Characteristics," Journal of Ship Research, Vol 17, No. 1, March, 1973.

27. Nancy Groves, "An Integral Prediction Method for Three-Dimensional Turbulent Boundary Layers on Rotating Blades," Paper presented at "Propellers '81 Symposium," SNAME, May, 1981.

APPENDIX – STREAMLINE COORDINATE SYSTEM

It is often convenient to have an orthogonal coordinate system on the surface of the blade. In particular, for performing boundary-layer computations, an orthogonal coordinate system with one variable along the streamlines reduces the number of terms in the governing equations. To determine the differential equation of the streamline path, let

$$x_R = \psi(x_c) \tag{120}$$

be the radius of the streamlines as a function of the chordwise coordinate x_c. Then

$$\underline{s}^*(x_c) = \underline{s}(x_c, \psi(x_c)) \tag{121}$$

is the position vector of the streamlines on the blade surface. Hence a tangent to the streamline is

$$\underline{t}_\psi = \frac{d\underline{s}^*}{dx_c} = \left(\frac{\partial \underline{s}}{\partial x_c}\right)_{x_R=\psi} + \left(\frac{\partial \underline{s}}{\partial x_R}\right)_{x_R=\psi} \cdot \frac{d\psi}{dx_R}$$

$$= D\left[\frac{c}{D}\underline{e}_1 + \left(\alpha \underline{e}_1 + \frac{\underline{N}_o^+ \times \underline{e}_1}{D^2 \frac{c}{D}}\right)\frac{d\psi}{dx_R}\right] \tag{122}$$

$$= D\left[\left(\frac{c}{D} + \alpha\frac{d\psi}{dx_c}\right)\underline{e}_1 + \frac{1}{2}\sqrt{1+N_{R_o}^2}\,\frac{d\psi}{dx_c}\,\hat{\underline{e}}\right]$$

For this tangent vector to be parallel to the velocity vector on the surface, the vector cross product, $\underline{t}_\psi \times \underline{q}$, must be zero. Hence, for the velocity on the blade surface given by

$$\frac{\underline{q}}{V} = \frac{\underline{q}_\infty}{V} + \frac{\underline{v}}{V}$$

$$= \frac{U}{V}\underline{e}_1 + \frac{W}{V}\hat{\underline{e}} \tag{123}$$

the cross product is

$$\frac{\underline{t}_\psi}{D} \times \frac{\underline{q}}{V} = \left\{\left(\frac{c}{D} + \alpha\frac{d\psi}{dx_c}\right)\underline{e}_1 + \frac{\sqrt{1+N_{R_o}^2}}{2}\frac{d\psi}{dx_c}\hat{\underline{e}}\right\} \times \left\{\frac{U}{V}\underline{e}_1 + \frac{W}{V}\hat{\underline{e}}\right\}$$

$$= \left\{-\frac{1}{2}\sqrt{1+N_{R_o}^2}\,\frac{d\psi}{dx_c}\,\frac{U}{V} + \left(\frac{c}{D} + \alpha\frac{d\psi}{dx_c}\right)\frac{W}{V}\right\}\underline{n}$$

For this cross product to be zero, the slope of the streamline is

$$\frac{d\psi}{dx_c} = \frac{\frac{c}{D}\frac{W}{V}}{\frac{1}{2}\sqrt{1+N_{R_o}^2}\,\frac{U}{V} - \alpha\frac{W}{V}} \tag{124}$$

For lines along the surface which are normal to the streamlines, let

$$x_c = \kappa(x_R) \tag{125}$$

be the chordwise position as a function of radius. Then a vector on the blade surface tangent to this line is

$$\underline{t}_n = \frac{d\underline{s}(\kappa(x_R), x_R)}{dx_R}$$

$$= \left(\frac{\partial \underline{s}}{\partial x_c}\right)_{x_c=\kappa}\frac{d\kappa}{dx_R} + \left(\frac{\partial \underline{s}}{\partial x_R}\right)_{x_c=\kappa} \tag{126}$$

$$= D\left[\frac{c}{D}\underline{e}_1\frac{d\kappa}{dx_R} + \alpha\underline{e}_1 + \frac{1}{2}\sqrt{1+N_{R_o}^2}\,\hat{\underline{e}}\right]$$

The condition to be satisfied is that $\underline{t}_n$ be perpendicular to the velocity vector, or

$$\frac{\underline{t}_n}{D} \cdot \frac{\underline{q}}{V} = 0 \tag{127}$$

$$= \frac{U}{V}\left(\frac{c}{D}\frac{d\kappa}{dx_R} + \alpha\right) + \frac{1}{2}\sqrt{1+N_{R_o}^2}\,\frac{W}{V} \tag{128}$$

Thus the slope of lines on the surface which are normal to the streamline is:

$$\frac{d\kappa}{dx_R} = -\frac{\frac{1}{2}\sqrt{1+N_{R_o}^2}\,\frac{W}{V} + \alpha\frac{U}{V}}{\frac{c}{D}\frac{U}{V}} \tag{129}$$

One now has differential equations to determine an orthogonal network over the blade surface. The differential arc length along the streamlines is

$$d\underline{s} = \left\{\left(\frac{\partial \underline{s}}{\partial x_c}\right)_{x_R=\psi} + \left(\frac{\partial \underline{s}}{\partial x_R}\right)_{x_R=\psi}\frac{d\psi}{dx_c}\right\}dx_c \tag{130}$$

Since

$$ds = |d\underline{s}| = h_1\,dx_c \tag{131}$$

then

$$h_1 = \left| \left(\frac{\partial \underline{s}}{\partial x_c} \right)_{x_R = \psi} + \left(\frac{\partial \underline{s}}{\partial x_R} \right)_{x_R = \psi} \frac{d\psi}{dx_c} \right|$$

or

$$\frac{h_1}{D} = \left\{ \left(\frac{c}{D} + \alpha \frac{d\psi}{dx_c} \right)^2 + \frac{1 + N_{R_o}^2}{4} \left(\frac{d\psi}{dx_c} \right)^2 \right\}^{1/2} \tag{132}$$

Similarly the differential arc length along the orthogonal surface coordinate is

$$ds = \left| \left(\frac{\partial \underline{s}}{\partial x_c} \right)_{x_c = \kappa} \frac{d\kappa}{dx_R} + \left(\frac{\partial \underline{s}}{\partial x_R} \right)_{x_c = \kappa} \right| dx_R \tag{133}$$

$$= h_2 \, dx_R \tag{134}$$

where

$$\frac{h_2}{D} = \left\{ \left(\frac{c}{D} \frac{d\kappa}{dx_R} + \alpha \right)^2 + \frac{1 + N_{R_o}^2}{4} \right\}^{1/2} \tag{135}$$

INITIAL DISTRIBUTION

Copies	
1	ARMY CHIEF OF RES & DIV
1	ARMY ENGR R&D LAB
2	CHONR
	1 Code 438
	1 LIB
1	NRL
4	ONR BOSTON
4	ONR CHICAGO
4	ONR LONDON, ENGLAND
2	USNA
	1 LIB
	1 Johnson
1	NAVPGSCOL LIB
1	NROTC & NAVADMINU, MIT
1	NADC
5	NOSC
	1 1311 LIB
	1 6005
	1 13111 LIB
	1 2501/Hoyt
	1 Nelson
1	NWC
38	NAVSEA
	1 SEA 032
	1 SEA 0321
	1 SEA 03D
	1 SEA 052
	1 SEA 052P
	3 SEA 0521
	1 SEA 0522
	3 SEA 0524
	1 SEA 0525
	3 SEA 05D
	3 SEA 05H
	5 SEA 05R
	1 PMS 378
	1 PMS 380
	1 PMS 381
	1 PMS 383
	1 PMS 389
	1 PMS 391
	1 PMS 392
	1 PMS 393
	1 PMS 397
	1 PMS 399
	1 PMS 400
	1 SEA Tech Rep Bath, England
	2 DET Norfolk (Sec 6660)
1	FAC 032C
1	MILITARY SEALIFT COMMAND (M-4EX)
1	NAVSHIPYD/PTSMH
1	NAVSHIPYD/PHILA
1	NAVSHIPYD/NORVA
1	NAVSHIPYD/CHASN
1	NAVSHIPYD/LBEACH
1	NAVSHIPYD/MARE
1	NAVSHIPYD/PUGET
1	NAVSHIPYD/PEARL
12	DTIC
2	HQS COGARD
1	U.S. COAST GUARD (G-ENE-4A)
1	LC/SCI & TECH DIV
8	MARAD
	1 DIV SHIP DES
	1 COORD RES
	1 Schubert
	1 Falls
	1 Dashnaw

Copies	
	1 Hammer
	1 Lasky
	1 Siebold
2	MMA
	1 LIB
	1 MARITIME RES CEN
2	NASA STIF
	2 DIR RES
1	NSF ENGR DIV LIB
1	DOT LIB
1	U BRIDGEPORT/URAM
2	U CAL BERKELY/DEPT NAME
	1 NAME LIB
	1 Webster
1	U CAL SAN DIEGO/Ellis
2	UC SCRIPPS
	1 Pollack
	1 Silverman
1	U MARYLAND/GLEN MARTIN INST
4	CIT
	1 AERO LIB
	1 Acosta
	1 Plesset
	1 Wu
1	CATHOLIC U
1	COLORADO STATE U/Albertson
1	U CONNECTICUT/Scottron
2	CORNELL U
	1 AERO DEPT
	1 THEOR APPL MECH DEPT
1	FLORIDA ATLANTIC U OE LIB

Copies	
1	FLORIDA STATE/OCEAN ENGR
1	HARVARD U
	1 MCKAY LIB
	1 Birkoff
	1 Carrier
2	U HAWAII/Bretschneider
1	U HOUSTON/Dalton
1	U ILLINOIS/Robertson
2	U IOWA
	1 IHR/Kennedy
	1 IHR/Landweber
2	JOHNS HOPKINS U
	1 Phillips
	1 INST COOP RES
1	U KANSAS CIV ENGR LIB
1	KANSAS ST U ENGR EXP/LIB
1	LEHIGH U FRITZ ENGR LAB LIB
1	LONG ISLAND U
4	U MICHIGAN
	1 NAME/LIB
	1 NAME/Ogilvie
	1 NAME/Vorus
	1 NAME/Latorre
6	MIT
	1 BARKER ENGR LIB
	1 OCEAN ENGR/Kerwin
	1 OCEAN ENGR/Leehey
	1 OCEAN ENGR/Newman
	1 OCEAN ENGR/Burke
	1 OCEAN ENGR/Van Houton
3	U MINNESOTA SAFHL
	1 Killen
	1 Song
	1 Wetzel

Copies	
1	U MISSISSIPPI, ME DEPT/Fox
1	NOTRE DAME ENGR LIB
5	PENN STATE U/ARL 1 LIB 1 Parkin 1 Henderson 1 Gearhart 1 Thompson
1	PRINCETON U/Mellor
1	RENSSELAER/MATH DEPT
3	SIT DAVIDSON LAB 1 LIB 1 Breslin 1 Tsakonas
1	STANFORD U/Ashley
1	STANFORD RES INST LIB
2	STATE U MARITIME COLL S U ARL LIB 1 ENGR DEPT 1 INST MATH SCI
1	ST JOHNS U
3	SWRI 1 APPLIED MECH REVIEW 1 Abramson 1 Burnside
1	TEXAS U ARL LIB
1	UTAH STATE U/Jeppson
3	WEBB INST 1 LIB 1 Ward 1 Hadler
1	WHOI OCEAN ENGR DEPT
1	WPI ALDEN HYDR LAB LIB
1	ASME/RES COMM INFO

Copies	
1	ASNE
1	SNAME
1	AERO JET-GENERAL/LIB
1	ALLIS CHALMERS, YORK, PA
1	AVCO LYCOMING
1	BAKER MANUFACTURING
2	BATH IRON WORKS CORP 1 Hansen 1 FFG PROJECT OFFICE
1	BETHLEHEM STEEL SPARROWS
3	BIRD-JOHNSON CO 1 Case 1 Ridley 1 Norton
1	BOEING ADV AMR SYS DIV
2	BOLT BERANEK AND NEWMAN 1 Brown 1 Jackson
1	BREWER ENGR LAB
1	CAMBRIDGE ACOUS/Junger
1	CALSPAN, INC/Ritter
2	DOUGLAS AIRCRAFT 1 TECH LIB 1 Smith
2	EXXON RES DIV 1 LIB 1 Fitzgerald
1	FRIEDE & GOLDMAN/Michel
1	GEN DYN CONVAIR ASW-MARINE SCIENCES

Copies	
3	GIBBS & COX 1 TECH LIB 1 Olson 1 CAPT Nelson
1	GRUMMAN AEROSPACE/Carl
3	HYDRONAUTICS 1 Etter 1 Scherer 1 LIB
3	HYDRODYNAMICS RESEARCH ASSOCIATES, INC. 1 Cox 1 Valentine 1 Nelka
1	INGALLS SHIPBLDG
1	INST FOR DEFENSE ANAL
1	LITTLETON R & ENGR CORP/Reed
1	LITTON INDUSTRIES
1	LOCKHEED/Waid
1	MARITECH, INC/Vassilopoulis
1	NATIONAL STEEL & SHIPBLDG
1	NEWPORT NEWS SHIPBLDG LIB
1	NIELSEN ENGR/Spangler
4	ORI, INC 1 Kim 1 Schneider 1 Williams 1 Kobayashi
1	HYDROMECHANICS, INC/Kaplin
1	NAR SPACE/Ujihara
1	PROPULSION DYNAMICS, INC
1	PROPULSION SYSTEMS, INC

Copies	
1	SCIENCE APPLICATIONS, INC/Stern
1	GEORGE G. SHARP
1	SPERRY SYS MGMT LIB/Shapiro
2	SUN SHIPBLDG 1 LIB 1 Neilson
1	ROBERT TAGGART
1	TETRA TECH PASADENA/Chapkis
1	TRACOR
1	UA HAMILTON STANDARD/Cornell

CENTER DISTRIBUTION

Copies	Code	Name
1	11	Ellsworth
1	1102.1	Nakonechny
1	15	Morgan
1	1509	Powell
1	152	Lin
1	1521	Day
1	1522	Wilson
1	1522	Dobay
1	1528	Reed
1	154	McCarthy
1	1543	Cumming
40	1544	Brockett
1	1544	Boswell
1	1544	Jessup
1	1544	Larimer
1	1552	Lee
1	1552	Libby
1	1556	Santore
1	1556	Coder
1	1556	Jeffers

CENTER DISTRIBUTION (Continued)

Copies	Code	Name
1	172	Krenzke
1	1720.6	Rockwell
1	19	Sevik
1	19	Strasberg
1	1903	Chertock
1	1962	Zaloumis
1	1962	Noonan
1	2814	Czyryca
10	5211.1	Reports Distribution
1	522.1	Library (C)
1	522.2	Library (A)

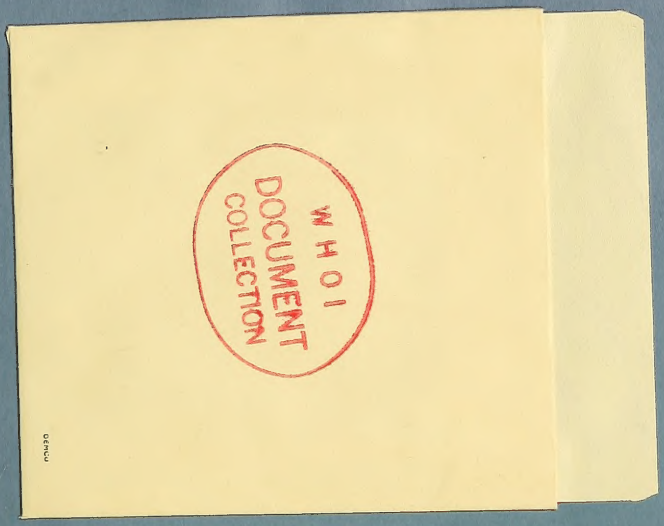

DTNSRDC ISSUES THREE TYPES OF REPORTS

1. DTNSRDC REPORTS, A FORMAL SERIES, CONTAIN INFORMATION OF PERMANENT TECHNICAL VALUE. THEY CARRY A CONSECUTIVE NUMERICAL IDENTIFICATION REGARDLESS OF THEIR CLASSIFICATION OR THE ORIGINATING DEPARTMENT.

2. DEPARTMENTAL REPORTS, A SEMIFORMAL SERIES, CONTAIN INFORMATION OF A PRELIMINARY, TEMPORARY, OR PROPRIETARY NATURE OR OF LIMITED INTEREST OR SIGNIFICANCE. THEY CARRY A DEPARTMENTAL ALPHANUMERICAL IDENTIFICATION.

3. TECHNICAL MEMORANDA, AN INFORMAL SERIES, CONTAIN TECHNICAL DOCUMENTATION OF LIMITED USE AND INTEREST. THEY ARE PRIMARILY WORKING PAPERS INTENDED FOR INTERNAL USE. THEY CARRY AN IDENTIFYING NUMBER WHICH INDICATES THEIR TYPE AND THE NUMERICAL CODE OF THE ORIGINATING DEPARTMENT. ANY DISTRIBUTION OUTSIDE DTNSRDC MUST BE APPROVED BY THE HEAD OF THE ORIGINATING DEPARTMENT ON A CASE-BY-CASE BASIS.